HHS Public Access

Author manuscript

Prog Neurobiol. Author manuscript; available in PMC 2022 April 01.

Published in final edited form as:

Prog Neurobiol. 2021 April ; 199: 101963. doi:10.1016/j.pneurobio.2020.101963.

Activation of endothelial Wnt/β-catenin signaling by protective astrocytes repairs BBB damage in ischemic stroke

Shanshan Song[1,2], **Huachen Huang**[1], **Xiudong Guan**[1], **Victoria Fiesler**[1,2], **Mohammad Iqbal H. Bhuiyan**[1,2], **Ruijia Liu**[1], **Shayan Jalali**[1], **Md Nabiul Hasan**[1,2], **Albert K Tai**[3], **Ansuman Chattopadhyay**[4], **Srilakshmi Chaparala**[4], **Ming Sun**[5], **Donna B. Stolz**[5], **Pingnian He**[6], **Dritan Agalliu**[7], **Dandan Sun**[1,2,8], **Gulnaz Begum**[1,2,*]

[1]Department of Neurology, University of Pittsburgh, Pittsburgh, PA, USA

[2]The Pittsburgh Institute for Neurodegenerative Diseases, University of Pittsburgh, Pittsburgh, PA, USA

[3]Department of Immunology, Tufts University, Boston, MA, USA

[4]Molecular Biology-Information Service, Health Sciences Library System, University of Pittsburgh, Pittsburgh, PA, USA

[5]Department of Cell Biology, University of Pittsburgh, Pittsburgh, PA, USA

[6]Department of Cellular and Molecular Physiology, Pennsylvania State University, College of Medicine, Hershey, PA, USA

[7]Departments of Neurology, Pathology & Cell Biology, Columbia University Irving Medical Center; New York, NY, USA

[8]Veterans Affairs Pittsburgh Health Care System, Geriatric Research, Educational and Clinical Center, Pittsburgh, PA, USA.

Abstract

The role of astrocytes in dysregulation of blood-brain barrier (BBB) function following ischemic stroke is not well understood. Here, we investigate the effects of restoring the repair properties of astrocytes on the BBB after ischemic stroke. Mice deficient for NHE1, a pH-sensitive Na^+/H^+ exchanger 1, in astrocytes have reduced BBB permeability after ischemic stroke, increased angiogenesis and cerebral blood flow perfusion, in contrast to wild-type mice. Bulk RNA-sequencing transcriptome analysis of purified astrocytes revealed that ~177 genes were differentially upregulated in mutant astrocytes, with *Wnt7a* mRNA among the top genes. Using a

[*]**Address correspondence to:** Gulnaz Begum, Ph.D., Department of Neurology, University of Pittsburgh, BST3-7018, 3501 5th Ave., Pittsburgh, PA 15260, USA, Tel: (608) 770-7446, gub6@pitt.edu/begumg@upmc.edu.

Author contributions: G.B. and D.S. conceived and designed the study, and planned and supervised the project. G.B., S.S., H.H., X.G., M.I.B., R.J., A.K.T., S.J., and M.S., performed research; G.B., and S.S., analyzed the data; G.B. D.A. and D.S., wrote the paper.

Declaration of Competing Interest

Authors declare no conflict of interests.

Wnt reporter line, we confirmed that the pathway was upregulated in cerebral vessels of mutant mice after ischemic stroke. However, administration of the Wnt/β-catenin inhibitor, XAV-939, blocked the reparative effects of *Nhe1*-deficient astrocytes. Thus, astrocytes lacking pH-sensitive NHE1 protein are transformed from injurious to "protective" by inducing Wnt production to promote BBB repair after ischemic stroke.

Graphical Abstract

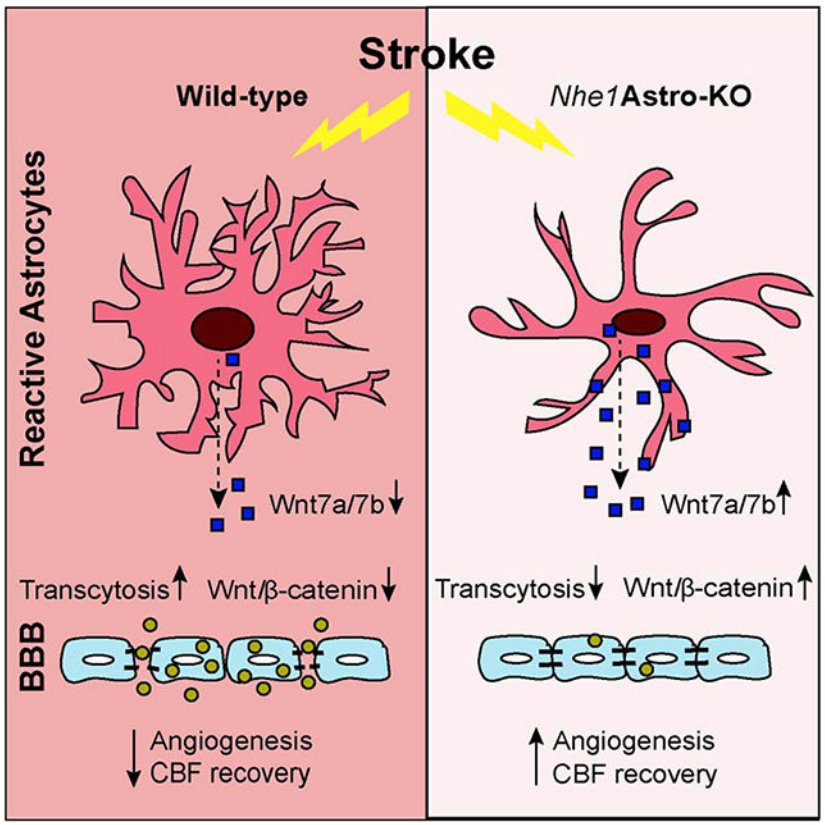

Keywords

Angiogenesis; Blood-Brain Barrier; Na^+/H^+ exchanger isoform-1; Astrocytes; Wnt/β-catenin signaling

INTRODUCTION

The crosstalk between endothelial cells (ECs), perivascular astrocytes, and pericytes plays an important role in regulating blood-brain barrier (BBB) maturation and integrity, which is essential for the central nervous system (CNS) homeostasis and function (Daneman and Engelhardt, 2017; Liebner et al., 2018; Weiss et al., 2009). Astrocytic endfeet cover ~99% of the cerebrovascular surface and regulate BBB integrity and cerebral blood flow (Iadecola and Nedergaard, 2007; Masamoto et al., 2015). Astrocytic endfeet are highly enriched in gap junction proteins such as connexin, aquaporin 4 (AQP4), and Kir4.1 channels and thus serve as specialized dynamic sites to regulate ion and water flow, which are essential for BBB

function (Alvarez et al., 2013; Boulay et al., 2016). Astrocyte-derived trophic factors, such as vascular endothelial growth factor (VEGF), basic fibroblast growth factor (bFGF), glial-derived neurotrophic factor (GDNF), angiopoitein-1 (ANG-1) etc., promote polarization of ECs and BBB maturation and maintenance (Abbott et al., 2006). Ischemic injury to the brain causes perivascular astrocytes to become reactive with altered functions. Perivascular reactive astrocytes display swollen endfeet and retract processes from blood vessels, resulting in opening of gap junctions and disassembly of endothelial tight junction (TJ) proteins leading to BBB damage (Haley and Lawrence, 2017; Xiang et al., 2016). Reactive astrocytes also release vascular permeability factors such as matrix metalloproteinases, nitric oxide, glutamate, and endothelin-1, which enhance BBB permeabilty (Michinaga and Koyama, 2019). Thus, the structural and functional changes in reactive astrocytes disrupt the astrocyte-EC interactions and fail to protect ECs and BBB function following brain injury (Abbott et al., 2006; Eilam et al., 2018). Therefore, restoring astrocyte function to re-establish their normal interactions with ECs is essential to decrease BBB damage and promote its repair after brain injury.

Wnt/β-catenin signaling is fundamental in CNS vascularization, BBB formation, and maturation during embryonic and postnatal development (Daneman et al., 2009; Liebner et al., 2008; Stenman et al., 2008). Wnt ligands, mainly secreted from astrocytes, neurons and oligodendrocytes, bind to Frizzled/LRP-5/6 receptor complexes on ECs to stabilize and activate cytosolic β-catenin (Hermann and ElAli, 2012; Zhou et al., 2014). Although that Wnt/β-catenin signaling is essential for maintenance of BBB integrity in adult brain (Wang et al., 2012), its role in neurovascular repair after ischemic injury has not been fully evaluated. Recent studies indicate that Wnt/β-catenin is dysregulated after stroke. Reduced nuclear β-catenin levels and loss of TJ protein claudin-1 were detected in the ECs of human brains in hemorrhagic stroke (Tran et al., 2016). Pharmacological inhibition of Wnt/β-catenin signaling, conditional knockout of the endothelial Gpr124 receptor, a co-activator of Wnt/β-catenin signaling, or Sox17, a downstream transcription factor, aggravate BBB breakdown and lead to hemorrhagic transformation in mouse brains after ischemic stroke (Chang et al., 2017; Corada et al., 2019; Jean LeBlanc et al., 2019). In contrast, pharmacological or genetic activation of Wnt/β-catenin signaling in *Gpr124*$^{-/-}$ mice rescued BBB disruption and hemorrhagic defects following ischemic stroke (Chang et al., 2017; Wang et al., 2017). Thus, Wnt/β-catenin signaling plays a crucial role in maintaining the BBB integrity in the adult brain after ischemic stroke.

We recently reported that selective deletion of astrocytic *Nhe1* in *Gfap-Cre*$^{ERT2+/-}$; *Nhe1*$^{f/f}$(*Nhe1* Astro-KO) mice abolished ischemic stroke-mediated astrogliosis and preserved BBB function (Begum et al., 2018). However, the molecular mechanisms underlying these protective effects are not well understood. In this study, we show that *Nhe1* Astro-KO mice have decreased transcellular and paracellular BBB leakage, increased angiogenesis and cerebral perfusion after ischemic stroke. These result from activation of Wnt/β-catenin signaling pathway in cerebral vessels of ischemic peri-lesion areas from astrocyte-derived Wnt7a. Our findings demonstrate that targeting astrocytic NHE1 protein or modulating its gene activity is a novel approach to transform abnormal astrocyte function into a more protective role for cerebral vascular repair following ischemic stroke.

2. MATERIAL AND METHODS

2.1. Chemicals

5-Bromo-2'-Deoxyuridine (BrdU), Tamoxifen, XAV-939, DAPI (4',6-Diamidino-2-Phenylindole, Dihydrochloride) were from Sigma-Aldrich (St. Louis, MO). Osmium Tetroxide and Uranyl Acetate were from Electron Microscopy Sciences (Hatfield, PA). Propylene oxide, Polybed 812 epoxy resin were from Polysciences (Warrington, PA). Toluidine Blue and Potassium Ferricyanide was from Fischer chemicals. Biocytin TMR (5-(and-6)-Tetramethylrhodamine Biocytin) and Albumin Alexa 488 were from Thermoscientific Life Technologies Corporation, (Grand Island, NY). iTaq™ Universal SYBR® Green, and iScript cDNA kit, were from Bio-rad laboratories (Hercules, CA), Rneasy Micro Kit was from Qiagen (Valencia, CA, USA D). Adult Brain Dissociation Kit, mouse and rat, Anti-ACSA-2 MicroBead Kit, mouse CD31 MicroBeads, mouse CD45 MicroBeads were from Miltenyi Biotec (Germany). DAB Peroxidase (HRP) Substrate Kit was from Vector Laboratories (CA).

2.2. Antibodies

Anti-Glucose Transporter (GLUT1) [SPM498] (ab40084), Sheep anti-BrdU, anti-mouse Serum Albumin were from Abcam (Cambridge, MA). Rabbit anti-Aquaporin 4 (AB3594) antibody was from Milipore (Billerica, MA). Mouse anti-Wnt-7a/b (H-8) sc 365459, and mouse anti-β-catenin (H-1) (sc-133240) antibodies were from Santa Cruz Biotechnology (Santa Cruz, CA). Goat anti-Rabbit IgG (H+L) Alexa Fluor 488, Goat anti-Rabbit IgG (H +L) Alexa Fluor 546, Donkey anti-Sheep IgG (H+L) Alexa Fluor 488 were from Thermoscientific Life Technologies Corporation (Grand Island, NY).

2.3. Animals

Nhe1$^{f/f}$ mice and *Gfap-Cre*$^{ERT2+/-}$*;Nhe1*$^{f/f}$ mice were established as described previously (Begum et al., 2018). *TCF/LEF*::H2B-eGFP; *Gfap-Cre*$^{ERT2+/-}$*;Nhe1*$^{f/f}$ double transgenic were created by crossing of *TCF/LEF*::H2B-eGFP reporter mice (Stock No: 013752 ; Jackson Laboratory) with *Nhe1*$^{f/f}$ mice to generate *TCF/LEF::H2B-eGFP;Nhe1*$^{f/f}$ mice. The subsequent crosses with *Gfap-Cre*$^{ERT2+/-}$*;Nhe1*$^{f/f}$ mice generated *TCF/LEF::H2B-eGFP; Gfap-CreERT2*$^{+/-}$*;Nhe1*$^{f/f}$ mice. PCR genotyping analysis was performed with genomic DNA of tail biopsies. Astrocyte specific deletion of *Nhe1 in Gfap-Cre*$^{ERT2+/-}$*;Nhe1*$^{f/f}$ mice (*Nhe1* Astro-KO) or in the double transgenic mice was induced by tamoxifen (Tam) (75 mg/kg/day in corn oil, i.p. for 5 days) starting at postnatal days 60 to 90 (P60-90). *Gfap-Cre*$^{ERT2+/-}$*;Nhe1*$^{f/f}$ mice receiving corn oil injections were served as controls (wild-type). A total of 110 male and female mice (3-4 months old) were used in the study. Animals were provided with food and water *ad libitum* and maintained in a temperature-controlled environment in a 12/12 h light-dark cycle. All studies were in compliance with the guidelines outlined in the Guide for the Care and Use of Laboratory Animals from the U.S. Department of Health and Human Services and were approved by the University of Pittsburgh Medical Center Institutional Animal Care and Use Committee. Surgeries and all outcome assessments were performed by investigators blinded to mouse genotype and experimental group assignments.

2.4. Focal ischemic stroke model

Transient focal cerebral ischemia was induced by intraluminal occlusion of left middle cerebral artery (MCA), as previously described (Begum et al., 2015). Briefly, under 1.5% isoflurane, the left common carotid artery (CCA) was exposed via a midline pre-tracheal incision and the external carotid artery (ECA) and the CCA were ligated. To occlude the MCA, a rubber silicon-coated monofilament suture (Filament size 6-0, diameter with coating 0.21 ± 0.02 mm; coating length 5 mm) was inserted into the ECA and advanced along the internal carotid artery 8-9 mm from the bifurcation of the carotid artery. For reperfusion, the suture was gently withdrawn 60 min after ischemia. Rectal temperature probes were inserted and body temperatures were maintained at 36.5±0.5 °C throughout the experiment by a heating blanket. Post-surgery mice were monitored at least once per day, and softened chew and water were provided during the first week post-surgery to accelerate recovery.

2.5. Regional cerebral blood flow (rCBF) measurements

Cerebral blood flow of the MCA areas was measured using a two-dimensional laserspeckle contrast analysis system (PeriCam PSI High Resolution with PIMSoft; Perimed, Jarfalla, Sweden) as described previously (Begum et al., 2018). Mice were anesthetized with isofluorane and maintained at physiological body temperature. The skull of the animal was secured in a stereotacticframe (David Kopf Instruments, Tujunga, CA). A midline incision was made in the scalp and the skull surface was cleaned with sterile normal saline. A charged-coupled device camera was placed 10 cm above the skull using a Pericam PSI System and blood perfusion images were taken at 5 min prior to MCAO, 5 min during MCAO and at 5 and 14 days reperfusion. Raw speckle images were taken in a 1.6 cm X 1.4 cm field (at 19 frames/s). Fifty-seven frames averaging, with the resolution of 0.02 mm^3 consecutive images at each time point per animal were averaged for analysis using equal-sized, oval-shaped regions of interest (ROI) covering the frontal and parietal bone plates of the ipsilateral (IL) and contralateral (CL) hemispheres of the wild-type and *Nhe1*-Astro KO mice. Cerebral blood perfusion is expressed in arbitrary units (perfusion units). Survival rates for wild-type and *Nhe1* Astro-KO mice are 100% and all animals have been included for rCBF analysis.

2.6. Immunofluorescent staining and image analysis

Mice were anesthetized and transcardially perfused as previously described (Begum et al., 2018). Coronal brains sections (25 μm, at −0.38 mm bregma) were washed with PBS and incubated with blocking solution (10% normal goat serum (NGS), 0.5% Triton X-100 in 0.1 M PBS) for 1 h at room temperature (RT) followed by incubation with primary antibodies: anti-Wnt7a/7b (1:200), anti-AQP4 (1:200), anti-Glut1 (1:200), anti-β-catenin (1:200), and anti-BrdU (1:100). All the primary antibodies were diluted in the blocking solution (3% NGS and 0.3% Triton X-100 in PBS) and incubated with brain sections overnight at 4 °C. On the following day, the sections were washed with PBS and then incubated with respective secondary Alexa 488/546 conjugated IgGs. DAPI (1:1000 in blocking solution) was used to stain the nucleus. For negative controls, brain sections were stained with the secondary antibody only or with IgG isotype control antibodies (Supplementary Fig. 1 and

2). Fluorescent images were captured with Olympus IX81 inverted microscope with a FV1000 laser scanning confocal system using a 40x oil-immersion objective and 1024 × 1024 pixel resolution (0.103 μm/pixel).

2.7. BrdU immunostaining analysis

To label newly synthesized DNA, mice received injections of 5-bromo-2-deoxyuridine (BrdU, 50 mg/kg in saline, i.p.) with an initial dose at day 3 after tMCAO and daily until sacrifice. Mice were sacrificed 2 h after the last BrdU injection at day 5 or day 14 after tMCAO. BrdU immunostaining of the brain sections was performed by pretreating the samples with 2 N HCL for 30 min at 37° C followed by 3 washes in 0.1 M PBS. Polyclonal sheep anti-BrdU (1:50) and mouse anti-Glut1 (1:200) were used for staining, followed by incubation of Alexa 546 donkey anti-sheep (1:200) or Alexa 488 donkey antimouse (1:200), respectively. Peri-infarct regions in the wild-type and *Nhe1* Astro-KO brains were identified as zone bordeing the infarct area (~450 μm from the border of the ischemic core) where necrotic tissue was absent (2,3,5-triphenyltetrazolium chloride (TTC) stained brain image in Figure 1). Per coronal section, a set of 3-4 1024×1024 images were collected from the peri-infarct spanning cortex and striatum. Samples in the CL hemispheres were taken homotopic to those collected in the IL regions. Fluorescent images were captured under 20× or 40× lens using Olympus IX81 inverted confocal laser scanning microscope. Identical digital imaging acquisition parameters were used throughout the study. Angiogenesis in the peri-infarct region was evaluated by counting the number of Glut1/BrdU double positive cells in a blinded manner using Fiji software.

2.8. Biocytin-TMR and IgG leakage quantitation

Following 12 or 48 h of Rp, 1% biocytin-TMR (100 μl) was injected into wild-type or *Nhe1* Astro-KO through tail vein. 30-45 min after injection, transcardial perfusion was performed with PBS followed by 4% paraformaldehyde (PFA). Brains were harvested, post-fixed with 4% PFA in PBS overnight, and sectioned in 25 μm-thick coronal slices with a Leica cryostat. Streptavidin-Alexa594 (1:100) was used to visualize biocytin-TMR distribution in tissues (Daneman et al., 2009). Sections were imaged with a NIKON Ti-E fluorescence microscope or Olympus IX81 confocal microscope. Biocytin leakage was quantified with Fiji software. Average intensity values for biocytin-TMR were measured by selecting identical regions in ipsilateral or contralateral cortices.

2.9. Albumin leakage quantitation

Following 6, 24 or 48 h of Rp, 1% albumin-Alexa488 was injected into wild-type or *Nhe1* Astro-KO through tail vein. 30-45 min after injection, brains were harvested as described above, and coronal slices were stained with fluorescent antibodies against Glut-1 (1:200) to visualize brain vasculature. Sections were imaged with an Olympus IX81 confocal microscope microscope. Glut-1 or albumin staining in cerebral blood vessels was automatically thresholded and separated from non-vasculature staining with the magic wand tool of Fiji software. Punctate albumin uptake in endothelial cells was then automatically thresholded. The vasculature area determined by Glut-1 staining was overlaid onto the albumin field of view in order to quantify endothelial cell-specific albumin endocytosis. The area of albumin endocytosis was calculated as percentage of blood vessel associated albumin

versus the total vasculature area in the image. “To validate that the albumin measured is indeed located within the endothelium, we performed 3D image analysis of alb-Alexa 488 and Glut1 immunostained stacked images using NIS elements software (NIKON). By using the “Binary operations” function, the alb Alexa 488^+ puncta present only in the $Glut1^+$ vessels were created. The 3D measurement analysis function on these overlaid images measured the volume of alb Alexa 488^+ puncta specific to $Glut1^+$ areas”.

2.10. Transmission electron microscopy (TEM)

TEM was performed as desribed previously (Begum et al., 2018). Briefly, mice were transcardially perfused with PBS followed by fixation with 2.5% glutaraldehyde for 24 h. After fixation, the brain was sectioned into 1 mm thick slices and post fixed in 2.5% glutaraldehyde in PBS. Under a dissection microscope, tissue punches were taken to capture the IL and CL peri-infarct areas in the cortex. Tissues were washed three times in PBS then, post-fixed in 1% osmium tetroxide with 1% potassium ferricyanide for 1 h. Following three additional PBS washes, the pellet was dehydrated through a graded series of 30-100% ethanol, 100% propylene oxide and then infiltrated in 1:1 mixture of propylene oxide: Polybed 812 epoxy resin for 1 h. After several changes of 100% resin over 24 hrs, pellet was embedded in a final change of resin, cured at 37°C overnight, followed by additional hardening at 65°C for two more days. Ultrathin (70 nm) sections were collected on 200 mesh copper grids, stained with 2% uranyl acetate in 50% methanol for 10 minutes, followed by 1% lead citrate for 7 min. Sections were imaged using a JEOL JEM 1011 transmission electron microscope (Peabody, MA) at 80 kV fitted with a side mount AMT 2k digital camera (Advanced Microscopy Techniques, Danvers, MA).

2.11. Isolation of astrocyte cell surface antigen-2 $(ACSA2)^+$ astrocytes and $CD31^+$ endothelial cells by magnetic-activated cell sorting (MACS)

Single cell suspension of astrocytes from the IL and CL hemispheres from wild-type and *Nhe1* Astro-KO brains were prepared using Adult Brain Dissociation Kit (Miltenyi Biotec, Germany) following manufacturers’ protocol. At 24 h post-tMCAO, brains were removed and placed in D-PBS (ice cold, pH 7.2). Cortex and striatum tissues were rapidly dissected on ice and separated in enzyme mixture with gentleMACS Octo Dissociator for 1 h at 37 °C. Digested tissues were dissociated into single cell suspension by filtration through 70 μm MACS SmartStrainer and a series of centrifugation steps as per manufacturers protocol. A total of ~ $2x10^6$ cells were used for isolation of astrocytes by magnetic bead seperation using anti-ASCA-2 microbead kit. For endothelial cell seperation, cells were first depleted of $CD45^+$ cells by incubating with CD45 microbeads for 15 min at 4 °C followed by seperation on a LD column. The $CD45^-$ effluent fraction was used to isolate $CD31^+$ cells. Cells were incubated with FcR blocking reagent for 10 min at 4 °C followed with a second incubation with anti-CD31 beads for 15 min at 4 °C. The cells were then washed in PEB buffer (D-PBS, and 0.5% bovine serum albumin), centrifuged at 300xg and resuspended in PEB buffer. The cell suspension was applied to the MS column, which was washed with 1-2 ml of PEB buffer and the eluted fraction was pelleted at 300xg for 10 min and ~200 μl of RLT buffer (Qiagen, Valencia, CA, USA) was added and stored at −80 °C untill analysis.

2.12. ACSA-2$^+$ cell RNA extraction, library preparation, and Illumina sequencing

RNA from ACSA-2$^+$ astrocytes was extracted on the QIAsymphony SP (Qiagen Corporation, Germany) using the QIAsymphony RNA Kit (Qiagen, 931636) and the protocol DNF-472T33 - HS Total RNA 15nt.mthds. The resulting RNA was eluted with RNase free water and stored at −80°C. Total RNA (500 ng) was used as input for library preparation. Three biological replicates for ACSA-2$^+$ astrocytes isolated from CL and IL ischemic hemispheres were sequenced on an Illumina HiSeq 2500 using High Output V4 chemistry and single read 100 bases format.

2.13. Bioinformatic data analysis

RNA-Seq data were analyzed using CLC genomics Workbench 10.1.1 (CLC bio, Aarhus, Denmark) following manufacturer's instruction. Briefly, single-end RNA-Seq reads, obtained in FASTQ format, were subjected to sequence quality checks using "QC for Sequencing Reads" tool. The reads were mapped against the mouse reference genome mm10 using default parameters of "RNA-Seq Analysis" tool. Genes and transcripts annotations provided by Ensembl_(release V86) were used. Diferentially expressed genes (DEGs) were identified between wild-type and *Nhe1* Astro-KO ischemic astrocyte samples using "Differential Expressions in Two Group" tool. The tool uses a multifactorial statistics based on a negative binomial Generalized Linear Model. Genes with FDR corrected P-value ≤ 0.05 and Log2 fold change ≤ 1.2 or ≤ −1.2 were considered as differentially expressed. The genes that were consistently induced or repressed in the three replicates were reported. Pathway enrichment analyses were generated through the use of QIAGEN's Ingenuity Pathway Analysis (IPA®, QIAGEN Redwood City, www.qiagen.com/ingenuity). Gene ontology (GO) analyses were applied for the functional annotation and pathway analysis, using the Database for Annotation Visualization and Integrated Discovery (DAVID; https://david.ncifcrf.gov/) (Huang da et al., 2009). The mouse genome was selected as the background parameter. P<0.05 and a count ≥2 were set as the thresholds to indicate a statistically significant difference. The RNA-Seq data have been deposited to the Gene Expression Omnibus (GEO) database with experiment series accession number [**GSE 145839**].

2.14. RT-qPCR analysis

MACS-isolated astrocytes or cerebral ECs were lysed in Qiagen RLT buffer, and RNA was extracted using the RNeasy Micro kit (Qiagen, 74134) following the manufacturer's instructions. RNA quantification was carried out by measuring absorbance with spectrophotometer ND-1000 (NanoDrop). Reverse transcription was performed using the iScript Reverse Transcription Supermix (Bio-Rad, 1708840) according to the manufacturer's protocol. All RNA isolated from cell pellets was converted into cDNA. Quantitative RT-PCR was performed using iTaq Universal SYBR Green Supermix (Bio-Rad, 172-5120) on a CFX 96 Touch Real-Time PCR Detection System. All relative gene expression analyses were performed using the 2–ΔΔCt method in a minimum of four animals per group with duplicate reactions for each gene evaluated. Following primer sequences were used: β-catenin, forward: GTACGCACCATGCAGAATAC, reverse: TGGAGCAGGAGATTATGCAG; Wnt7a, forward: CTG TGG CTG CGA CAA GGA GA, reverse: TGG CAC GCA CAG

GCT CCA CGT GG, Wnt7b forward: GGT GTG GCA GTG TAC CTG CAA, Wnt7b reverse: GTG AAG ACC TCG GTG CGC T. GAPDH forward: AAC TTT GGC ATT GTG GAA GG, reverse: ACA CAT TGG GGG TAG GAA CA; 18S forward: GTAACCCGTTGAACCCCATT, 18S reverse: CCATCCAATCGGTAGTAGCG.

2.15. Histology for hemorrhagic transformation

Endogenous peroxidase activity was used to visualize hemorrhagic transformation through reaction with diaminobenzidine (DAB) without prior treatment with hydrogen peroxide (Fernandez-Lopez et al., 2016). Brain sections were washed and stained in DAB/H2O2 solution for 10 min, and washed again. Slices were mouted onto slides, dried, and overlaid with coverslips using distyrene plasticizer zylene (DPX) mounting solutions. Images were captured using NIKON Ti microscope equipped with a color camera. The percent of hemorrhagic areas was quantified in the ipsilateral and contralateral hemispheres in 4 serial sections per brain (~500 μm apart), covering the rostrocaudal extent of the infarct.

2.16. Statistical analysis

Data was graphed using GraphPad Prism, version 4 (GraphPad Software, Inc., San Diego, CA) or Sigma plot (Systat Software Inc. San Jose, CA). Student's two-tailed t test was used for comparison of two experimental groups. For three or more groups, multiple comparisons were done using two-way or three-way ANOVA where appropriate followed by appropriate post-hoc comparison tests for multiple pairwise examinations. Outliers were identified if they were below or above 1.5 times the interquartile range. Changes were identified as significant if P value was less than 0.05. Mean values were reported together with the standard error of mean (SEM) or standard deviation (SD).

3. RESULTS

3.1. *Nhe1* Astro-KO mice displayed enhanced angiogenesis and cerebral perfusion after ischemic stroke

We have previously shown that selective reduction of NHE1 protein in $GFAP^+$ astrocytes (*Nhe1* Astro-KO brains) abolished ischemic stroke-mediated astrogliosis and preserved BBB function (Begum et al., 2018). To investigate these mechanisms in detail, we evaluated changes in BBB integrity and cerebral vessel repair in wild-type and *Nhe1* Astro-KO mice after ischemic stroke (Fig. 1A). We first assessed the impact of deletion of astrocytic *Nhe1* on angiogenesis by analyzing the density of $BrdU^+/Glut1^+$ cerebral vessels of wild-type and *Nhe1* Astro-KO brains post-stroke (Fig. 1B, C). *Nhe1* Astro-KO brains exhibited significantly higher $BrdU^+/Glut1^+$ ECs (~2-fold increase) in the peri-lesion cortical tissues compared to the corresponding regions in the contralateral (CL) hemispheres than the wild-type brains at both, day 5 ($p<0.05$) and 14 ($p<0.05$) post-stroke (Fig. 1B, C). We then evaluated the outcome of increased angiogenesis on cerebral perfusion by measuring longitudinal changes of regional cerebral blood perfusion (rCBF) in both wild-type and *Nhe1* Astro-KO mice prior to and during transient middle cerebral artery occlusion (tMCAO) induction, as well as at day 5 and 14 of reperfusion using a PeriCam PSI System imager with a speckle laser. tMCAO induced a significant reduction in the rCBF in the CL hemispheres in the wild-type brains but not the *Nhe1* Astro-KO brains (65.30 ± 6.08 vs.

85.93 ± 6.70 %, $p < 0.05$) (Fig. 1D, E), which was sustained during 14 days post-tMCAO. Both wild-type and *Nhe1* Astro-KO mice displayed a significant decrease (~50%) in the rCBF in the ipsilateral (IL) hemispheres immediately upon tMCAO induction (Fig. 1D, E). However, compared to the wild-type mice, the *Nhe1* Astro-KO mice showed persistent faster rCBF recovery in the IL hemispheres at day 5-14 post-stroke, ($p < 0.01$). In contrast, the IL rCBF of wild-type mice remained at 60.3 ± 4.4% of baseline during 14-day post-stroke ($p < 0.001$). These findings suggest that *Nhe1* Astro-KO mice exhibited increased angiogenesis leading to better recovery of the cerebral perfusion post-MCAO.

We have perviously shown that selective deletion of *Nhe1* in Astro-KO mice does not alter astrocyte morphology and GFAP protein expression in non-lesioned brain tissues (Begum et al., 2018). We further detected similar abundant S100 β expression, a calcium binding protein mainly expressed by astrocytes in the healthy brains, in non-ischemic hemispheres of the wild-type and *Nhe1* Astro-KO brains (Supplementary Fig. 3A, B). Moreover, there were no differences in perivascular astrocyte morphology, perivascular astrogliosis, blood vessel morphology or BBB permeability to serum albumin between wild-type or *Nhe1* Astro-KO naïve mice (Supplementary Fig. 3C-E). These data clearly demonstrate that selective deletion of *Nhe1* in astrocytes does not significantly alter perivascular astrocyte or BBB properties in *Nhe1* Astro-KO naïve brains.

3.2. *Nhe1* Astro-KO mice exhibited reduced paracellular and transcellular BBB permeability after ischemic stroke

Ischemia-mediated cerebral EC dysfunction causes disruption of rCBF and BBB damage (Hu et al., 2017). Increased paracellular leakage due to disruption of endothelial TJs and transcellular permeability due to upregulation of caveolae are two important cell biological mechanisms of BBB dysfunction after ischemic stroke (Haley and Lawrence, 2017; Knowland et al., 2014). First, we examined time-dependent changes in endothelial transcytosis of fluorescently labeled albumin (alb-Alexa488) in wild-type and *Nhe1* Astro-KO brains after ischemic stroke. Mice were injected with 1% alb-Alexa 488 and the amount of alb-Alexa 488 present in the cerebral ECs was measured at various time points. No alb-Alexa 488^+ fluorescence signals were detected in either of the two groups at 6 h post reperfusion. At 24 h post reperfusion, there was a ~10 % increase in the alb-Alexa 488^+ vesicles in $Glut1^+$ ECs in IL peri-lesion areas of wild-type brains, which remained elevated at 48 h post-stroke (Fig. 2A, B). In contrast, the *Nhe1* Astro-KO brains exhibited significantly lower amount of alb-Alexa 488^+ vesicles in ECs located within IL peri-lesions at 24 (2.7 ± 1.6% $p < 0.05$) as well as at 48 hours after reperfusion (3.4 ± 2.0%, $p < 0.05$). 3D image analysis also indicated the increased presence of alb-Alexa 488^+ vesicles in the endothelium of wild-type brains (Supplementary Fig. 4). To further confirm that increased alb-Alexa 488^+ vesicles reflect changes in endothelial transcytosis, we examined the density of intracellular vesicles in cerebral ECs by transmission electron microscopy (TEM) (Villasenor et al., 2019). A significantly higher number of endothelial vesicles was detected in IL peri-lesion areas of wild-type brains at 24 h post-stroke (47 ± 9.3 vs 19.2 ± 2.1, $p < 0.05$) compared to *Nhe1* Astro-KO brains (Fig. 2C; arrows). Very few vesicles were detected in ECs in the CL hemispheres (cortex/striatum) in both groups (Fig. 2D). We also performed immunostaining of cerebral vessels with an additional EC marker, tomato lectin. Similar to

Glut1$^+$ ECs, an ~8 % increase in the alb-Alexa 488$^+$ vesicles were detected in tomato lectin$^+$ ECs in IL peri-lesion areas of wild-type brains. However, in *Nhe1* Astro-KO brains, the alb-Alexa 488$^+$ vesicles in tomato lectin$^+$ ECs remained low (2.3 ±1.3 %)" (Supplementary Fig. 5). Therefore, ischemic stroke stimulates endothelial transcytosis and impairs BBB in the wild-type brains; in contrast, *Nhe1* Astro-KO brains show reduced transcytosis in CNS ECs after ischemic stroke.

Following stroke, loss of endothelial TJ integrity can lead to increased paracellular BBB permeability. We assessed chages in paracellular BBB permeability in the ischemic hemispheres of wild-type and *Nhe1* Astro-KO brains by analyzing extravasation of a low molecular weight tracer, 5-(and-6-) tetramethylrhodamine biocytin (biocytin-TMR) following tMCAO. Biocytin-TMR crosses the BBB only when paracellular permeability is enhanced and can be used as a marker for paracellular leakage (Knowland et al., 2014; Lengfeld et al., 2017; Lutz et al., 2017). Biocytin-TMR average pixel intensities were increased in the IL peri-lesion areas of wild-type brains at 48 h reperfusion (Fig. 2E, F; arrows). Compared to wild-type brains, *Nhe1* Astro-KO brains showed a significant decrease in biocytin-TMR leakage at 48 h reperfusion (0.8 ± 0.7 vs 10.6 ± 2.8) (Fig. 2E, F). We further evaluated the expression of the endothelial tight junction protein claudin-5 in cerebral vessels of wild-type and *Nhe1* Astro-KO brains at 48 h after ischemic stroke (Supplementary Fig. 6). The abundant expression of endothelial claudin-5 was detected in cerebral vessels of the healthy CL regions in both groups. However, the IL regions of wild-type brains displayed reduced claudin-5 expression with discontinuous distribution patterns (Supplementary Fig. 6, arrowhead). In contrast, no loss of claudin-5 expression was detected in *Nhe1* Astro-KO brains (Supplementary Fig. 6, arrow), suggesting that tight junctions were intact. These data suggest that deletion of astrocytic *Nhe1* reduces BBB damage by maintaining paracellular barrier at acute stages of ischemic stroke.

3.3. *Nhe1* Astro-KO mice upregulate Wnt/β-catenin signaling gene signature after ischemic stroke

To investigate the molecular mechanisms underlying astrocyte-mediated BBB protection and improved cerebral perfusion in *Nhe1* Astro-KO mice, we characterized transcriptome profiles of astrocytes isolated from either wild-type or *Nhe1* Astro-KO brains at 24 h post tMCAO. The purity of astrocytes isolated through MACS was confirmed by expression of gene markers specifically enriched in astrocytes (*Gfap, Aldh1l1, Aqp4, and Slc2a1*) but not well-established for other CNS cell types (Supplementary Fig. 7A-E). Specifically, no markers for neurons and trace levels of specific marker genes for oligodendrocytes, ECs or pericytes were detected.

The bulk RNAseq analysis identified 340 genes that were differentially expressed in *Nhe1* KO compared to WT astrocytes (Fig. 3B). Among these genes, 177 genes were upregulated, and 163 genes were downregulated in *Nhe1*-deleted astrocytes (Fig. 3C, D). *Gdf1, Hes5, Prss56, Wnt7a, Sprr1a, and Rph3a* are among the top 10 most up-regulated mRNAs (Supplementary Fig. 8). These genes primarily encode for signaling molecules or growth factors involved in cellular differentiation and developmental processes (Ahmed et al., 2009; Andersson et al., 2006). Compared to healthy astrocytes, ischemic astrocytes from wild-type

brains showed a significantly reduced expression of both *Wnt7a* and *Wnt7b* genes (Supplementary Fig. 9). In contrast, only *Wnt7a* but not *Wnt7b* mRNA expression was significantly reduced in ischemic astrocytes from *Nhe1* Astro-KO brains. Notably, *Wnt7a* and *Wnt7b* transcripts were significantly upregulated in ischemic *Nhe1* KO astrocytes (Fig. 3D), which was accompanied by upregulation of several additional genes in the Wnt pathway (*Fzd9, and Fzd10*). The hierarchical clustering analysis of gene expression changes further revealed a clear separation between the two groups and specific transcriptome signatures for *Nhel*-deleted astrocytes (Fig. 3C, D). The enrichment analysis by gene ontology (GO) using DAVID software showed that these genes are involved in "nervous system development", "ion transport", "establishment of the blood-nerve barrier", "canonical Wnt signaling", and "cell proliferation" ($p < 0.05$) (Supplementary Fig. 10). Wnt/β-catenin pathway was also among the most significantly changed pathways identified by the Ingenuity Pathway Analysis (IPA) (Fig. 3E). This pathway is known to regulate BBB maturation and CNS vascular repair in traumatic brain injury, multiple sclerosis, Huntington's disease and stroke (Chang et al., 2017; Lengfeld et al., 2017; Lim et al., 2017; Salehi et al., 2018). These data suggest that upregulated Wnt/β-catenin signaling in *Nhe1* Astro-KO brains may have a causative role in BBB protection and vascular repair after ischemic stroke.

3.4. *Nhe1* Astro-KO mice displayed increased Wnt7a/7b expression after ischemic stroke

Next, we assessed changes of Wnt7a/7b mRNA and protein expression in wild-type and *Nhe1* Astro-KO brains. Immunofluorescence analysis detected abundant Wnt7a/7b protein in the cerebral vessels of CL hemispheres of both wild-type and *Nhe1* Astro-KO brains (Fig. 4A; arrows). At 48 h post-stroke, Wnt7a/7b proteins were decreased in cerebral vessels within the IL peri-lesion areas of the wild-type brains (Fig. 4A; arrowheads). In contrast, the *Nhe1* Astro-KO brains displayed preserved Wnt7a/7b expression in the IL perilesional vessels (Fig. 4A, B). This is consistent with qPCR analysis data, showing a significant increase in *Wnt7a* and *Wnt7b* mRNA in the astrocytes and ECs from the IL hemispheres of *Nhe1* Astro-KO, but not wild-type, brains (Fig. 4C and Supplementary Fig. 11). In addition, ECs from *Nhe1* Astro-KO ischemic brains showed a significant increase in *Wnt7a/7b* mRNA expression (Supplementary Fig. 11). Together, these results corroborate our RNAseq bioinformatics findings that upregulation of Wnt/β-catenin signaling in *Nhe1* Astro-KO mice is likely responsible for preserved BBB integrity and cerebral perfusion after ischemic stroke.

3.5. *Gfap-Cre$^{ERT2+/-}$;Nhe1$^{f/f}$* mice exhibit increased endothelial Wnt activity after ischemic stroke

Active β-catenin translocate to the nucleus and associates with TCF/LEF (T-cell factor/lymphoid enhancing factor) nuclear complex to induce expression of the BBB junctional proteins claudin-5 and occludin (Liebner et al., 2008; Taddei et al., 2008; Wang et al., 2020). To further ascertain that *Nhe1* Astro-KO brains upregulate Wnt/β-catenin pathway in cerebral vessels in response to ischemic stroke, we visualized changes in Wnt/β-catenin pathway activation by crossing *TCF/LEF*::H2B-eGFP,a Wnt reporter transgenic mouse line expressing a fusion of green fluorescent protein (eGFP) with histone H2B protein under the control of a β-catenin transcriptional target TCF/LEF1 response element (Ferrer-Vaquer et

al., 2010) to *G/ap-Cre*$^{ERT2+/-}$*;Nhe1*$^{f/f}$ mice (Fig. 5A). Reduced eGFP$^+$ nuclear signals were detected in the Glut1$^+$ cerebral ECs in IL peri-lesion areas of wild-type Wnt reporter brains at 24 h reperfusion (22.4 ± 2.3 %; $p<0.05$, Fig. 5B, C), indicating decreased Wnt activity. eGFP$^+$ signals were also detected in few Glut1$^-$ cells, indicating Wnt reporter activity in other cell types. In contrast, a significant increase in the eGFP$^+$ nuclear signals (33.1 ± 2.6 %; $p<0.05$) was detected in Glut1$^+$ cerebral ECs in the peri-lesion areas of *Nhe1* Astro-KO Wnt reporter brains at 24 h reperfusion (Fig. 5B; arrows). These findings are further supported by elevated β-catenin protein in *Nhe1* Astro-KO brains at 48 h post-stroke. β-catenin immunoreactivity was detected in the cerebral vessels in the CL hemisphere of both wild-type and *Nhe1* Astro-KO brains (Fig. 5D; arrows), with the predominant β-catenin signals located in the ECs of AQP4$^+$ vessels. However, the IL hemisphere of wild-type brains showed reduced β-catenin immunosignals in the cerebral vessels at the peri-lesion areas (Fig. 5D; arrowheads). In contrast, the peri-lesion vessels of *Nhe1* Astro-KO brains showed no loss of β-catenin expression (Fig. 5E). Our findings from these various approaches collectively demonstrate that *Nhe1* Astro-KO brains strongly upregulate Wnt/β-catenin signaling in ECs after ischemic stroke.

3.6. Wnt/β-catenin inhibitor XAV-939 increases vulnerability of Nhe1 Astro-KO brains to stroke-induced vascular injury

To assess the impact of elevated Wnt/β-catenin pathway on preserved BBB integrity in ischemic *Nhe1* Astro-KO brains, we tested whether inhibition of Wnt/β-catenin pathway with a small molecule inhibitor XAV-939, which selectively inhibits β-catenin-mediated transcription (Huang et al., 2009), could abolish the resistance of *Nhe1* Astro-KO brains to ischemic damage. Vehicle (DMSO) or XAV-939 (40 mg/kg; i.p) was administered to either wild-type or *Nhe1* Astro-KO mice at 4 hours after reperfusion following ischemic stroke. By 24 h reperfusion, the vehicle-treated wild-type brains displayed a significant increase in parenchymal infiltration and cellular accumulation of serum albumin in the ischemic peri-lesion areas ($p < 0.05$) (Fig. 6A, B, arrows), a respective index for leaky BBB and neuronal degeneration and death (Maeda et al., 1992; Park et al., 2017). In comparison, vehicle-treated *Nhe1* Astro-KO brains showed significantly less parenchymal as well as cellular accumulation of albumin (Fig. 6A). No albumin leakage was detected in the sham brains or CL hemispheres of both groups (Supplementary Fig. 12). In contrast, XAV-939 treatment increased similarly albumin infiltration in the ischemic peri-lesion areas of both wild-type (30.0 ± 4.9 vs 23.6 ± 4.0; $p<0.05$) and *Nhe1* Astro-KO brains (25.8 ± 4.6 vs 11.6 ± 3.6; $p < 0.05$) (Fig. 6A, B). These data suggest that Wnt/β-catenin activation is required for preservation of BBB integrity in the *Nhe1* Astro-KO brains.

Disruption of BBB is central to hemorrhagic transformation after ischemic stroke. Interestingly, we observed that XAV-939 treatment increased the incidence of intracerebral hemorrhages in the ischemic parenchyma regions in the cortex and striatum of wild-type brains, as was evident from the presence of extravascular clusters of red blood cells (Fig. 6C). However, the number of hemorrhages in the XAV-939-treated *Nhe1* Astro-KO brains was lower (Fig. 6C, D). In addition, XAV-939 treatment did not increase the incidence of hemorrhages in the CL hemispheres of both genetic groups (Fig. 6D). Together, these results

demonstrate that Wnt/β-catenin pathway is vital for preserving BBB permeability of ischemic *Nhe1* Astro-KO brains.

4. DISCUSSION

In this study, we demonstrate that astrocyte-specific deletion of *Nhe1* reduces BBB damage and improves cerebral perfusion via stimulating Wnt/β-catenin signaling after ischemic stroke. NHE1 protein represents a major pathway for H^+ extrusion in exchange for Na^+ in astrocytes. Ischemia and cellular acidosis triggers sustained NHE1 activation resulting in Na^+ overload and astrocytic swelling in reactive astrocytes (Kintner et al., 2004). Reactive astrocytes become deregulated and lose their normal supportive functions essential for neuronal survival (Sofroniew, 2009). Recently, we reported that *Nhe1* gene deletion in $GFAP^+$ reactive astrocytes attenuated astrocytic hypertrophy, decreased infarct volume, and improved neurological functional recovery after ischemic stroke (Begum et al., 2018). We showed abundant NHE1 protein expression in both $GFAP^+$ astrocytes and neurons in the ischemic hemispheres of wild-type brains. NHE1 protein expression was absent in $GFAP^+$ astrocytes in the *Nhe1* Astro-KO brains and remained unchanged in neurons, indicating that *Nhe1* expression is specifically reduced in $GFAP^+$ astrocytes in *Nhe1* Astro-KO mice (Begum et al., 2018). In exploring the underlying mechanisms, here we demonstrate that selective deletion of *Nhe1* in astrocytes restores their reparative functions. Whole transcriptome analysis by RNA-Seq of wild-type and *Nhe1* Astro-KO astrocytes revealed that 340 genes were significantly different (Supplementary Fig. 8). Many of the genes that were upregulated are involved in supporting neuronal health. For example, *Gdf1*, *Cspg4, fut9, Hes5, Nrsn1, Wnt7a, Bdnf* etc. are important for BBB function, neuronal differentiation and survival. In contrast, astrocytic proinflammatory gene *Lcn2* (Bi et al., 2013) was selectively reduced in *Nhe1* Astro-KO astrocytes. Taken together, our study indicates that astrocytic NHE1 protein is involved in regulating astrocyte reactivity and function, deleting *Nhe1* restores astrocytic supportive and protective functions.

Nhe1 Astro-KO mice displayed better cerebral perfusion and BBB integrity after ischemic stroke

Our study illustrated that astrocyte specific deletion of *Nhe1* in $Gfap\text{-}Cre^{ERT2+/-};Nhe1^{f/f}$ mice significantly improved cerebral perfusion at 5 and 14 days after ischemic stroke, which was accompanied with enhanced post-ischemic angiogenesis by facilitating EC proliferation in the ischemic peri-lesion areas. We also detected higher rCBF in the CL hemispheres in the *Nhe1* Astro-KO brains than wild-type brains during 14 days post-tMCAO. The precise underlying mechanisms for the improved CL rCBF in *Nhe1* Astro-KO mice are not clear, but this is consistent with the phenomena that higher CBF in CL hemispheres is a predictor of better long-term clinical outcomes in post-stroke patients, possibly due to better collateral perfusion abilities (Thamm et al., 2019). In contrast to the increased paracellular and transcellular BBB leakage observed in the ischemic wild-type brains, *Nhe1* Astro-KO brains showed decreased paracellular BBB permeability at 48 hours post-stroke and a paralleled decrease in the rate of albumin transcytosis at 24-48 h post-stroke. Transcellular and paracellular routes both contribute to increased BBB permeability after ischemic stroke however, upregulation in transcytosis (transcellular route) is known to precede degradation

of tight junctions (paracellular route) (Knowland et al., 2014). We speculate that the reduced EC transcytosis in *Nhe1* Astro-KO brains could be due to reduced damage to ECs as well as increased vascular repair processes, which together preserve endothelial function. The lack of pericytes is also known to upregulate transcytosis (Armulik et al., 2010); we cannot exclude the possibility that *Nhe1*-deficient protective astrocytes also preserve the function of pericytes, which will be the focus of our future studies.

Vascular repair after ischemic stroke requires angiogenesis and regrowth of new blood vessels from the pre-existing vascular tree, which promote re-establishment of microcirculation to restore blood supply to the damaged tissues (Han et al., 2015; Navaratna et al., 2009; Zhang et al., 2014). While perivascular astrocytes play a critical function in vascular remodeling by providing pro-angiogenic growth factors for vessel repair (Alvarez et al., 2013; Morita et al., 2015), ischemic injury severely compromises these functions. In the *Nhe1* Astro-KO mice, we detected increased expression of Wnt7a/7b in ECs located within ischemic peri-lesion areas. Wnt7a/7b have been implicated in brain angiogenesis (Daneman et al., 2009; Liebner et al., 2008; Stenman et al., 2008) since genetic inactivation of Wnt7a and Wnt7b leads to severely defective CNS angiogenesis (Daneman et al., 2009; Stenman et al., 2008). Stroke impairs BBB properties ranging from neurovascular barrier integrity, pericyte coverage, tight junction protein production. These neurovascular abnormalities can be rescued by EC-specific activation of Wnt pathway via activated β-catenin (Chang et al., 2017). However, it is not completely understood how the pathway is regulated in brain ECs in response to ischemic stroke. Our study suggests that modulating reactive astrocytic function by deleting *Nhe1* can stimulate Wnt/β-catenin signaling in ECs via increased β-catenin expression which in-turn contributes to reduced vascular damage and increased vascular repair processes. Thus, we have uncovered a critical underlying and poorly understood cellular mechanism to prevent ischemic brain infarct and swelling, and improve motor sensory function outcomes in *Nhe1* Astro-KO mice at 1-7 days post-stroke (Begum et al., 2018).

Wnt/β-catenin signaling in cerebral vascular repair after ischemic stroke

In the adult brain cerebral cortex, Wnt7a/7b are the predominant Wnts secreted by astrocytes, oligodendrocytes, and neurons that activate endothelial β-catenin signaling pathway via Frizzled (Fzd) and LRP5/6 receptor complex (Hermann and ElAli, 2012; Zhou et al., 2014). The Wnt/β-catenin signaling pathway is robustly activated in cerebral vessels during development and declines in the adult brain; however its activity is essential to maintain BBB integrity in healthy CNS and after brain injury (Chang et al., 2017; Stenman et al., 2008; Tran et al., 2016). β-catenin is both an adherens junction protein linking to the actin cytoskeleton and a transcription factor central to the Wnt signaling pathway (Valenta et al., 2012). Studies show that constitutive endothelial β-catenin activity is required for the maintenance of BBB integrity via transcriptional control of expression of TJ proteins claudin-5 and occludin (Wang et al., 2020). The expression and localization of the TJ proteins directly correlates with BBB permeability (Krueger et al., 2013). Breakdown of TJs and increased paracellular permeability of the CNS endothelium occurs at the 24-48 h following ischemic stroke (Knowland et al., 2014). A recent study showed that expression of active β-catenin was increased predominately in brain ECs at 3 h after ischemic stroke and

declined thereafter (Jean LeBlanc et al., 2019); this may function as an intrinsic compensatory mechanism to restore BBB function. We detected significant decrease of Wnt7a/7b and β-catenin protein in ECs of wild-type brains at 48 h post-stroke, indicating sustained dysfunctional Wnt signaling in ischemic brains. However, we identified a key role for astrocytic Wnt7a/7b ligands in mediating astrocyte-EC interactions for maintaining BBB structural integrity after ischemic stroke. By RNA-Seq analysis, we detected a significant increase in Wnt7a/7b gene expression in astrocytes of *Nhe1* Astro-KO brains at 24 h post-stroke. This was accompanied with predominantly increased Wnt7a/7b and β-catenin protein expression in the cerebral ECs in ischemic peri-lesion areas of *Nhe1* Astro-brains. In brain ECs, β-catenin activation and subsequent translocation to the nucleus activate LEF/TCF transcription factor and specifically induce expression of the TJ proteins (Hermann and ElAli, 2012; Liebner et al., 2008). Using *TCF/LEF*::H2B-eGFP mice, enhanced Wnt reporter activity was only observed in the ischemic peri-lesion ECs of *Nhe1* Astro-KO double transgenic mice. These data, in corroboration with our biochemical findings, indicate that dysfunctional Wnt/β-catenin signaling pathway contributes to BBB damage after ischemic stroke.

Pharmacological inhibition of β-catenin signaling worsened ischemic BBB damage and increased intracerebral hemorrhages

The importance of astrocytic Wnt/β-catenin signaling in maintaining the integrity of BBB in *Nhe1* Astro-KO after ischemic stroke was further supported by our pharmacological study. Post-tMCAO administration of XAV-939, the selective inhibitor of β-catenin mediated transcription, worsened the BBB damage in the wild-type brains and abolished the protective effects in the *Nhe1* Astro-KO brains. These data support that astrocytic deletion of *Nhe1* increased resilience of the BBB in the *Nhe1* Astro-KO brains after ischemic stroke by enhancing the β-catenin signaling. In addition, we detected increased hemorrhages in the XAV-939-treated wild-type brains more than the *Nhe1* Astro-KO brains. The resistance to XAV-939-mediated BBB damage seen in *Nhe1* Astro-KO brains could be due to the incomplete blocking of Wnt signaling by XAV-939 since the levels of Wnt7a/7b protein expression are significantly higher in *Nhe1* Astro-KO brains compared to wild-type brains. Treatment with similar dose of XAV-939 immediately after MCAO induction has shown residual β-catenin protein expression in the isolated brain capillaries 24 h after stroke, suggesting for possible incomplete inhibition (Jean LeBlanc et al., 2019). We cannot rule out involvement of Wnt-independent mechanisms in resilience of *Nhe1* Astro-KO brains. Astrocyte secreted growth factors like FGF, and GDNF, are involved in maintaining as well as in promoting vascular integrity (Cabezas et al., 2016; Huang et al., 2012). We have found a significant increase in the expression of *Fgf, Bdnf* and *Pdgfa* genes in *Nhe1* Astro-KO brains (data not shown).

Hemorrhagic transformation after ischemic stroke can result from aggravated BBB breakdown due to the activation of reactive oxygen species (ROS) and matrix metalloproteinases (MMPs) (Jickling et al., 2014). In ischemic mouse brains, increase in superoxide and peroxynitrite radicals were detected in microvessels and astrocytic end-feet at 2 h reperfusion, which correlated with BBB damage (Gursoy-Ozdemir et al., 2004). Active MMP-mediated proteolysis has also been detected in ischemic leaking capillaries that

produce ROS (Gasche et al., 2001). Ischemia-induced MMPs are shown to act on the basal lamina to disrupt the endothelia-pericyte-astrocyte complex and facilitate BBB injury and promote hemorrhagic transformation (Wang and Shuaib, 2007). We recently reported decreased expression of MMP9 protein in astrocytic *Nhe1* KO brains at 48 h after ischemic stroke, indicating that astrocytic deletion of *Nhe1* ameliorates MMP9 secretion/activity upon ischemic stroke (Begum et al., 2018). Taken together, our data indicated that *Nhe1* Astro-KO brains could confer additional protection to stroke-induced BBB damage resulting from decreased MMP9 activity or ROS production in perivascular astrocytes. Further studies are needed to delineate these mechanisms in *Nhe1* Astro-KO brains to prevent hemorrhagic transformation after ischemic stroke.

5. CONCLUSIONS

Our findings demonstrate for the first time that astrocytes play a critical role in the regulation of Wnt/β-catenin signaling in the cerebral vessels. By using inducible, astrocyte specific *Gfap-CreER*$^{+/-}$*;Nhe1*$^{f/f}$ conditional knockout mice, we demonstrated that selective deletion of astrocytic *Nhe1* gene in astrocytes reduced endothelial transcytosis, basal endothelial vesicles and BBB damage after ischemic stroke. This was accompanied by increased expression of Wnt7a/7b proteins and preserved Wnt/β-catenin signaling in the ECs, resulting in increased vascular repair and improved CBF after ischemic stroke (Fig. 7). Treatment with β-catenin specific inhibitor XAV-939 abolished the BBB permeability protective effects in the *Nhe1* Astro-KO brains. These findings unravel the important roles of astrocytes in preserving the BBB integrity and cerebral perfusion via stimulating canonical Wnt/β-catenin signaling after ischemic stroke. Taken together, our results suggest that restoring astrocyte protective function by inhibition of astrocytic NHE1 activity accelerates neurovascular repair after ischemic injury via activation of Wnt/β-catenin signaling pathway.

Supplementary Material

Refer to Web version on PubMed Central for supplementary material.

Acknowledgements

This work was supported by NIH grants: NIH R01 NS048216 (D.S), NIH R01 NS110755-01A1 (G.B) and S10OD016236 (S.W).

REFERENCES

Abbott NJ, Ronnback L, Hansson E, 2006. Astrocyte-endothelial interactions at the blood-brain barrier. Nat Rev Neurosci 7, 41–53. [PubMed: 16371949]

Ahmed S, Gan HT, Lam CS, Poonepalli A, Ramasamy S, Tay Y, Tham M, Yu YH, 2009. Transcription factors and neural stem cell self-renewal, growth and differentiation. Cell Adh Migr 3, 412–424. [PubMed: 19535895]

Alvarez JI, Katayama T, Prat A, 2013. Glial influence on the blood brain barrier. Glia 61, 1939–1958. [PubMed: 24123158]

Andersson O, Reissmann E, Jornvall H, Ibanez CF, 2006. Synergistic interaction between Gdf1 and Nodal during anterior axis development. Dev Biol 293, 370–381. [PubMed: 16564040]

Armulik A, Genove G, Mae M, Nisancioglu MH, Wallgard E, Niaudet C, He L, Norlin J, Lindblom P, Strittmatter K, Johansson BR, Betsholtz C, 2010. Pericytes regulate the blood-brain barrier. Nature 468, 557–561. [PubMed: 20944627]

Begum G, Song S, Wang S, Zhao H, Bhuiyan MIH, Li E, Nepomuceno R, Ye Q, Sun M, Calderon MJ, Stolz DB, St Croix C, Watkins SC, Chen Y, He P, Shull GE, Sun D, 2018. Selective knockout of astrocytic Na(+) /H(+) exchanger isoform 1 reduces astrogliosis, BBB damage, infarction, and improves neurological function after ischemic stroke. Glia 66, 126–144. [PubMed: 28925083]

Begum G, Yuan H, Kahle KT, Li L, Wang S, Shi Y, Shmukler BE, Yang SS, Lin SH, Alper SL, Sun D, 2015. Inhibition of WNK3 Kinase Signaling Reduces Brain Damage and Accelerates Neurological Recovery After Stroke. Stroke 46, 1956–1965. [PubMed: 26069258]

Bi F, Huang C, Tong J, Qiu G, Huang B, Wu Q, Li F, Xu Z, Bowser R, Xia XG, Zhou H, 2013. Reactive astrocytes secrete lcn2 to promote neuron death. Proc Natl Acad Sci U S A 110, 4069–4074. [PubMed: 23431168]

Boulay AC, Cisternino S, Cohen-Salmon M, 2016. Immunoregulation at the gliovascular unit in the healthy brain: A focus on Connexin 43. Brain Behav Immun 56, 1–9. [PubMed: 26674996]

Cabezas R, Avila-Rodriguez M, Vega-Vela NE, Echeverria V, Gonzalez J, Hidalgo OA, Santos AB, Aliev G, Barreto GE, 2016. Growth Factors and Astrocytes Metabolism: Possible Roles for Platelet Derived Growth Factor. Med Chem 12, 204–210. [PubMed: 26477707]

Chang J, Mancuso MR, Maier C, Liang X, Yuki K, Yang L, Kwong JW, Wang J, Rao V, Vallon M, Kosinski C, Zhang JJ, Mah AT, Xu L, Li L, Gholamin S, Reyes TF, Li R, Kuhnert F, Han X, Yuan J, Chiou SH, Brettman AD, Daly L, Corney DC, Cheshier SH, Shortliffe LD, Wu X, Snyder M, Chan P, Giffard RG, Chang HY, Andreasson K, Kuo CJ, 2017. Gpr124 is essential for blood-brain barrier integrity in central nervous system disease. Nat Med 23, 450–460. [PubMed: 28288111]

Corada M, Orsenigo F, Bhat GP, Conze LL, Breviario F, Cunha SI, Claesson-Welsh L, Beznoussenko GV, Mironov AA, Bacigaluppi M, Martino G, Pitulescu ME, Adams RH, Magnusson P, Dejana E, 2019. Fine-Tuning of Sox17 and Canonical Wnt Coordinates the Permeability Properties of the Blood-Brain Barrier. Circ Res 124, 511–525. [PubMed: 30591003]

Daneman R, Agalliu D, Zhou L, Kuhnert F, Kuo CJ, Barres BA, 2009. Wnt/beta-catenin signaling is required for CNS, but not non-CNS, angiogenesis. Proc Natl Acad Sci U S A 106, 641–646. [PubMed: 19129494]

Daneman R, Engelhardt B, 2017. Brain barriers in health and disease. Neurobiol Dis 107, 1–3. [PubMed: 28552387]

Eilam R, Segal M, Malach R, Sela M, Arnon R, Aharoni R, 2018. Astrocyte disruption of neurovascular communication is linked to cortical damage in an animal model of multiple sclerosis. Glia 66, 1098–1117. [PubMed: 29424049]

Fernandez-Lopez D, Faustino J, Klibanov AL, Derugin N, Blanchard E, Simon F, Leib SL, Vexler ZS, 2016. Microglial Cells Prevent Hemorrhage in Neonatal Focal Arterial Stroke. JNeurosci 36, 2881–2893. [PubMed: 26961944]

Ferrer-Vaquer A, Piliszek A, Tian G, Aho RJ, Dufort D, Hadjantonakis AK, 2010. A sensitive and bright single-cell resolution live imaging reporter of Wnt/ss-catenin signaling in the mouse. BMC Dev Biol 10, 121. [PubMed: 21176145]

Gasche Y, Copin JC, Sugawara T, Fujimura M, Chan PH, 2001. Matrix metalloproteinase inhibition prevents oxidative stress-associated blood-brain barrier disruption after transient focal cerebral ischemia. J Cereb Blood Flow Metab 21, 1393–1400. [PubMed: 11740200]

Gursoy-Ozdemir Y, Can A, Dalkara T, 2004. Reperfusion-induced oxidative/nitrative injury to neurovascular unit after focal cerebral ischemia. Stroke 35, 1449–1453. [PubMed: 15073398]

Haley MJ, Lawrence CB, 2017. The blood-brain barrier after stroke: Structural studies and the role of transcytotic vesicles. J Cereb Blood Flow Metab 37, 456–470. [PubMed: 26823471]

Han L, Li J, Chen Y, Zhang M, Qian L, Chen Y, Wu Z, Xu Y, Li J, 2015. Human Urinary Kallidinogenase Promotes Angiogenesis and Cerebral Perfusion in Experimental Stroke. PLoS One 10, e0134543. [PubMed: 26222055]

Hermann DM, ElAli A, 2012. The abluminal endothelial membrane in neurovascular remodeling in health and disease. Sci Signal 5, re4. [PubMed: 22871611]

Hu X, De Silva TM, Chen J, Faraci FM, 2017. Cerebral Vascular Disease and Neurovascular Injury in Ischemic Stroke. Circ Res 120, 449–471. [PubMed: 28154097]

Huang B, Krafft PR, Ma Q, Rolland WB, Caner B, Lekic T, Manaenko A, Le M, Tang J, Zhang JH, 2012. Fibroblast growth factors preserve blood-brain barrier integrity through RhoA inhibition after intracerebral hemorrhage in mice. Neurobiol Dis 46, 204–214. [PubMed: 22300708]

Huang da W, Sherman BT, Lempicki RA, 2009. Systematic and integrative analysis of large gene lists using DAVID bioinformatics resources. Nat Protoc 4, 44–57. [PubMed: 19131956]

Huang SM, Mishina YM, Liu S, Cheung A, Stegmeier F, Michaud GA, Charlat O, Wiellette E, Zhang Y, Wiessner S, Hild M, Shi X, Wilson CJ, Mickanin C, Myer V, Fazal A, Tomlinson R, Serluca F, Shao W, Cheng H, Shultz M, Rau C, Schirle M, Schlegl J, Ghidelli S, Fawell S, Lu C, Curtis D, Kirschner MW, Lengauer C, Finan PM, Tallarico JA, Bouwmeester T, Porter JA, Bauer A, Cong F, 2009. Tankyrase inhibition stabilizes axin and antagonizes Wnt signalling. Nature 461, 614–620. [PubMed: 19759537]

Iadecola C, Nedergaard M, 2007. Glial regulation of the cerebral microvasculature. Nat Neurosci 10, 1369–1376. [PubMed: 17965657]

Jean LeBlanc N, Menet R, Picard K, Parent G, Tremblay ME, ElAli A, 2019. Canonical Wnt Pathway Maintains Blood-Brain Barrier Integrity upon Ischemic Stroke and Its Activation Ameliorates Tissue Plasminogen Activator Therapy. Mol Neurobiol 56, 6521–6538. [PubMed: 30852795]

Jickling GC, Liu D, Stamova B, Ander BP, Zhan X, Lu A, Sharp FR, 2014. Hemorrhagic transformation after ischemic stroke in animals and humans. J Cereb Blood Flow Metab 34, 185–199. [PubMed: 24281743]

Kintner DB, Su G, Lenart B, Ballard AJ, Meyer JW, Ng LL, Shull GE, Sun D, 2004. Increased tolerance to oxygen and glucose deprivation in astrocytes from Na(+)/H(+) exchanger isoform 1 null mice. Am J Physiol Cell Physiol 287, C12–21. [PubMed: 15013953]

Knowland D, Arac A, Sekiguchi KJ, Hsu M, Lutz SE, Perrino J, Steinberg GK, Barres BA, Nimmerjahn A, Agalliu D, 2014. Stepwise recruitment of transcellular and paracellular pathways underlies blood-brain barrier breakdown in stroke. Neuron 82, 603–617. [PubMed: 24746419]

Krueger M, Hartig W, Reichenbach A, Bechmann I, Michalski D, 2013. Blood-brain barrier breakdown after embolic stroke in rats occurs without ultrastructural evidence for disrupting tight junctions. PLoS One 8, e56419. [PubMed: 23468865]

Lengfeld JE, Lutz SE, Smith JR, Diaconu C, Scott C, Kofman SB, Choi C, Walsh CM, Raine CS, Agalliu I, Agalliu D, 2017. Endothelial Wnt/beta-catenin signaling reduces immune cell infiltration in multiple sclerosis. Proc Natl Acad Sci U S A 114, E1168–E1177. [PubMed: 28137846]

Liebner S, Corada M, Bangsow T, Babbage J, Taddei A, Czupalla CJ, Reis M, Felici A, Wolburg H, Fruttiger M, Taketo MM, von Melchner H, Plate KH, Gerhardt H, Dejana E, 2008. Wnt/beta-catenin signaling controls development of the blood-brain barrier. J Cell Biol 183, 409–417. [PubMed: 18955553]

Liebner S, Dijkhuizen RM, Reiss Y, Plate KH, Agalliu D, Constantin G, 2018. Functional morphology of the blood-brain barrier in health and disease. Acta Neuropathol 135, 311–336. [PubMed: 29411111]

Lim RG, Quan C, Reyes-Ortiz AM, Lutz SE, Kedaigle AJ, Gipson TA, Wu J, Vatine GD, Stocksdale J, Casale MS, Svendsen CN, Fraenkel E, Housman DE, Agalliu D, Thompson LM, 2017. Huntington's Disease iPSC-Derived Brain Microvascular Endothelial Cells Reveal WNT-Mediated Angiogenic and Blood-Brain Barrier Deficits. Cell Rep 19, 1365–1377. [PubMed: 28514657]

Lutz SE, Smith JR, Kim DH, Olson CVL, Ellefsen K, Bates JM, Gandhi SP, Agalliu D, 2017. Caveolin1 Is Required for Th1 Cell Infiltration, but Not Tight Junction Remodeling, at the Blood-Brain Barrier in Autoimmune Neuroinflammation. Cell Rep 21, 2104–2117. [PubMed: 29166603]

Maeda M, Akai F, Nishida S, Yanagihara T, 1992. Intracerebral distribution of albumin after transient cerebral ischemia: light and electron microscopic immunocytochemical investigation. Acta Neuropathol 84, 59–66. [PubMed: 1502882]

Masamoto K, Unekawa M, Watanabe T, Toriumi H, Takuwa H, Kawaguchi H, Kanno I, Matsui K, Tanaka KF, Tomita Y, Suzuki N, 2015. Unveiling astrocytic control of cerebral blood flow with optogenetics. Sci Rep 5, 11455. [PubMed: 26076820]

Michinaga S, Koyama Y, 2019. Dual Roles of Astrocyte-Derived Factors in Regulation of Blood-Brain Barrier Function after Brain Damage. Int J Mol Sci 20.

Morita S, Furube E, Mannari T, Okuda H, Tatsumi K, Wanaka A, Miyata S, 2015. Vascular endothelial growth factor-dependent angiogenesis and dynamic vascular plasticity in the sensory circumventricular organs of adult mouse brain. Cell Tissue Res 359, 865–884. [PubMed: 25573819]

Navaratna D, Guo S, Arai K, Lo EH, 2009. Mechanisms and targets for angiogenic therapy after stroke. Cell Adh Migr 3, 216–223. [PubMed: 19363301]

Park JH, Park JA, Ahn JH, Kim YH, Kang IJ, Won MH, Lee CH, 2017. Transient cerebral ischemia induces albumin expression in microglia only in the CA1 region of the gerbil hippocampus. Mol Med Rep 16, 661–665. [PubMed: 28586018]

Salehi A, Jullienne A, Baghchechi M, Hamer M, Walsworth M, Donovan V, Tang J, Zhang JH, Pearce WJ, Obenaus A, 2018. Up-regulation of Wnt/beta-catenin expression is accompanied with vascular repair after traumatic brain injury. J Cereb Blood Flow Metab 38, 274–289. [PubMed: 29160735]

Sofroniew MV, 2009. Molecular dissection of reactive astrogliosis and glial scar formation. Trends Neurosci 32, 638–647. [PubMed: 19782411]

Stenman JM, Rajagopal J, Carroll TJ, Ishibashi M, McMahon J, McMahon AP, 2008. Canonical Wnt signaling regulates organ-specific assembly and differentiation of CNS vasculature. Science 322, 1247–1250. [PubMed: 19023080]

Taddei A, Giampietro C, Conti A, Orsenigo F, Breviario F, Pirazzoli V, Potente M, Daly C, Dimmeler S, Dejana E, 2008. Endothelial adherens junctions control tight junctions by VE-cadherin-mediated upregulation of claudin-5. Nat Cell Biol 10, 923–934. [PubMed: 18604199]

Thamm T, Guo J, Rosenberg J, Liang T, Marks MP, Christensen S, Do HM, Kemp SM, Adair E, Eyngorn I, Mlynash M, Jovin TG, Keogh BP, Chen HJ, Lansberg MG, Albers GW, Zaharchuk G, 2019. Contralateral Hemispheric Cerebral Blood Flow Measured With Arterial Spin Labeling Can Predict Outcome in Acute Stroke. Stroke 50, 3408–3415. [PubMed: 31619150]

Tran KA, Zhang X, Predescu D, Huang X, Machado RF, Gothert JR, Malik AB, Valyi-Nagy T, Zhao YY, 2016. Endothelial beta-Catenin Signaling Is Required for Maintaining Adult Blood-Brain Barrier Integrity and Central Nervous System Homeostasis. Circulation 133, 177–186. [PubMed: 26538583]

Valenta T, Hausmann G, Basler K, 2012. The many faces and functions of beta-catenin. EMBO J 31, 2714–2736. [PubMed: 22617422]

Villasenor R, Lampe J, Schwaninger M, Collin L, 2019. Intracellular transport and regulation of transcytosis across the blood-brain barrier. Cell Mol Life Sci 76, 1081–1092. [PubMed: 30523362]

Wang CX, Shuaib A, 2007. Critical role of microvasculature basal lamina in ischemic brain injury. Prog Neurobiol 83, 140–148. [PubMed: 17868971]

Wang L, Geng J, Qu M, Yuan F, Wang Y, Pan J, Li Y, Ma Y, Zhou P, Zhang Z, Yang GY, 2020. Oligodendrocyte precursor cells transplantation protects blood-brain barrier in a mouse model of brain ischemia via Wnt/beta-catenin signaling. Cell Death Dis 11, 9. [PubMed: 31907363]

Wang W, Li M, Wang Y, Wang Z, Zhang W, Guan F, Chen Q, Wang J, 2017. GSK-3beta as a target for protection against transient cerebral ischemia. Int J Med Sci 14, 333–39. [PubMed: 28553165]

Wang Y, Rattner A, Zhou Y, Williams J, Smallwood PM, Nathans J, 2012. Norrin/Frizzled4 signaling in retinal vascular development and blood brain barrier plasticity. Cell 151, 1332–1344. [PubMed: 23217714]

Weiss N, Miller F, Cazaubon S, Couraud PO, 2009. The blood-brain barrier in brain homeostasis and neurological diseases. Biochim Biophys Acta 1788, 842–857. [PubMed: 19061857]

Xiang J, Tang Y, Li C, Su EJ, Lawrence DA, Keep RF, 2016. Mechanisms Underlying Astrocyte Endfeet Swelling in Stroke. Acta Neurochir Suppl 121, 19–22. [PubMed: 26463917]

Zhang RL, Chopp M, Roberts C, Liu X, Wei M, Nejad-Davarani SP, Wang X, Zhang ZG, 2014. Stroke increases neural stem cells and angiogenesis in the neurogenic niche of the adult mouse. PLoS One 9, e113972. [PubMed: 25437857]

Zhou Y, Wang Y, Tischfield M, Williams J, Smallwood PM, Rattner A, Taketo MM, Nathans J, 2014. Canonical WNT signaling components in vascular development and barrier formation. J Clin Invest 124, 3825–3846. [PubMed: 25083995]

Highlights

- Ischemic stroke triggers perivascular reactive asrocyte transfromation and BBB damage.
- Selective deletion of Na^+/H^+ exchanger I (NHE1) in astrocytes activates Wnt/β-catenin signaling pathway.
- Active Wnt/β-catenin signaling increases BBB integrity, and promotes cerebral vessel repair.

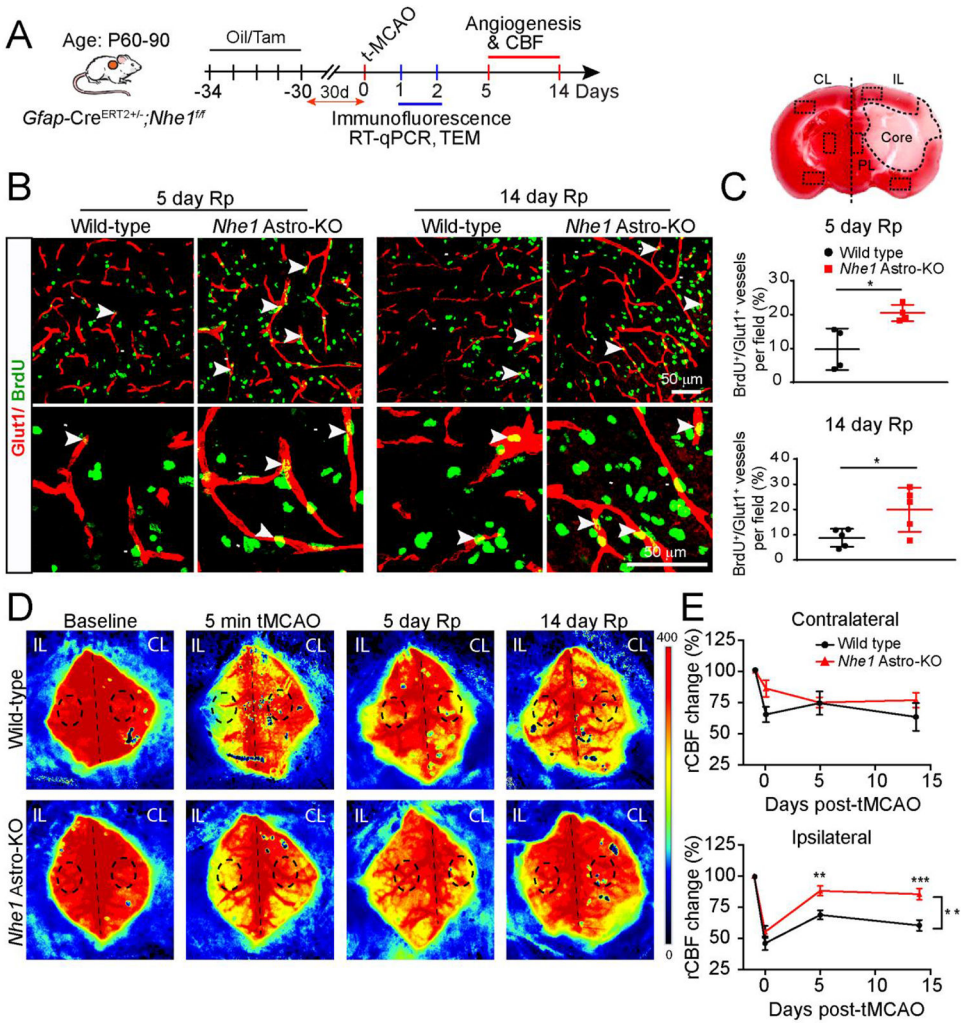

Fig. 1.

Nhe1 Astro-KO mice show increased angiogenesis and improved rCBF. (A) Experimental protocol. Gfap-CreER+/−;*Nhe1*f/f mice at postnatal days P60–90 were treated with either corn oil or tamoxifen (Tam) in corn oil (75 mg/kg/day, ip) for 5 days. After 30 days, ischemic stroke was induced by tMCAO at P90–120. Measurement of rCBF and biochemical assays were conducted in the CL or IL peri-lesion cortex and striatum. (B and C) Representative confocal images of BrdU+ and Glut1+ cerebral vessels in the peri-lesion areas at 5 or 14 days reperfusion (Rp) were shown and angiogenesis (Brdu+/Glut1+ double positive vessels) was quantified. Data are mean ± SEM, n = 4-5 *p < 0.05 (Student's t-test). (D and E) Representative images of Laser Speckle analysis of regional cerebral blood flow (rCBF) in the wild-type and *Nhe1* Astro-KO mice prior to tMCAO (baseline), at 5 min during tMCAO, at 5 days or 14 days of reperfusion. Black dashed circles indicate the regions of interest for quantification of blood perfusion in MCA regions. Pseudo color scale indicate red as high blood perfusion and blue as low blood perfusion. Summary analysis of rCBF changes as percentage of pre-ischemic baseline in CL and IL hemispheres. Data are mean ± SEM, n = 5. * p < 0.05, ** p < 0.01; *** p < 0.001 (two-way ANOVA followed by Sidak's multiple comparisons test).

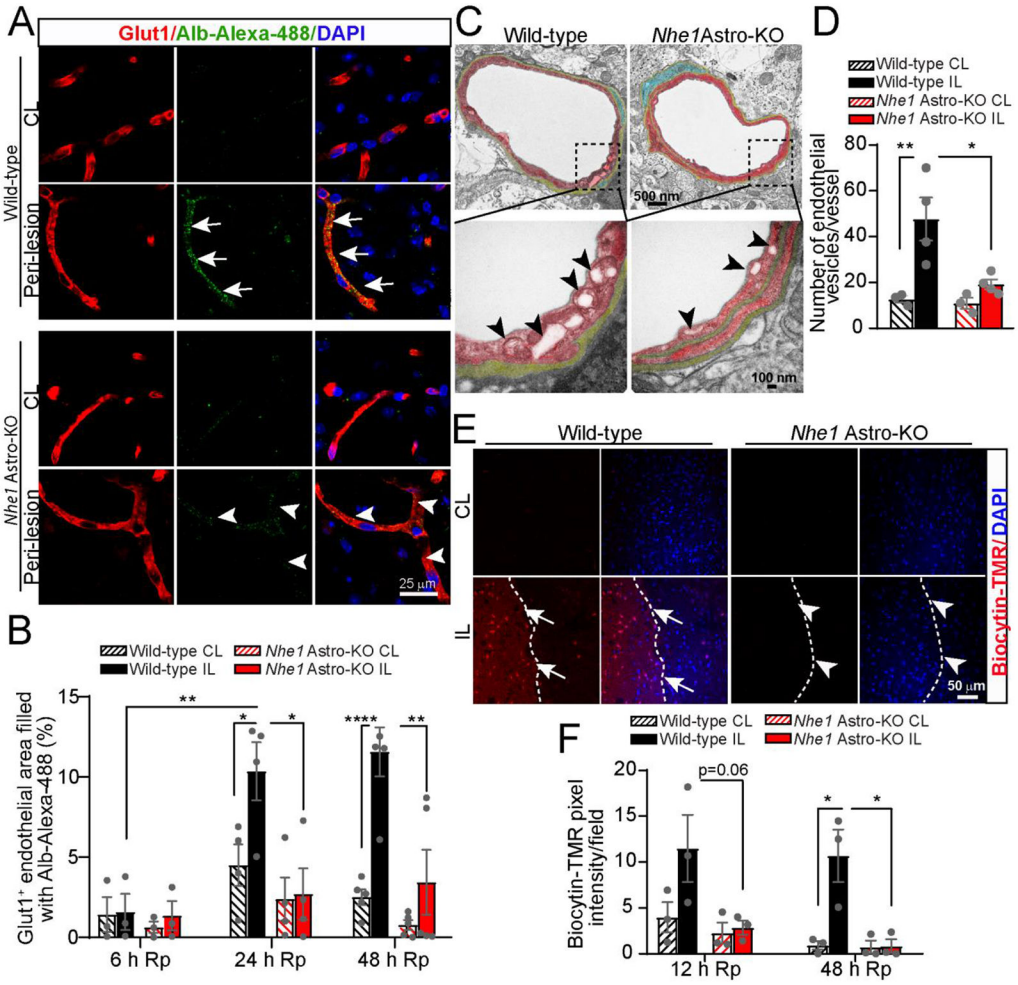

Fig. 2.

Nhe1 Astro-KO mice show reduced transcytosis and paracellular permeability after ischemic stroke. (A) Representative confocal images of alb-Alexa 488 labelled caveolae and other transcytosis vesicles in Glut1+ cerebral vessels of wild-type and *Nhe1*Astro-KO brains at 48 h Rp. (B) Quantification of Glut1+ endothelial area filled with alb-Alexa 488. Data are mean ± SEM, n = 3–5 animals per time point, *p<0.05; ** p < 0.01; ****p<0.0001 (three-way ANOVA followed by Tukey's multiple comparisons test). (C) Representative TEM images of cerebral vessels in the peri-infarct areas of wild-type and *Nhe1* Astro-KO brains at 24 h Rp. Arrows: endocytotic vesicles in the endothelial lumen. (D) Summary. Data are ± SEM, n = 3, *p < 0.05. (Student's t-test) (E) Confocal images of biocytin-TMR immunofluorescence in the IL peri-lesion areas. Arrows; increased tracer leakage in the parenchyma and neural cells. Arrow heads; reduced tracer leakage. (F) Bar graph represents the biocytin-TMR average pixel intensity in the IL peri-infarct and CL areas. Data are mean ± SEM, n = 3. * p<0.05; (three-way ANOVA followed by Tukey's multiple comparisons test).

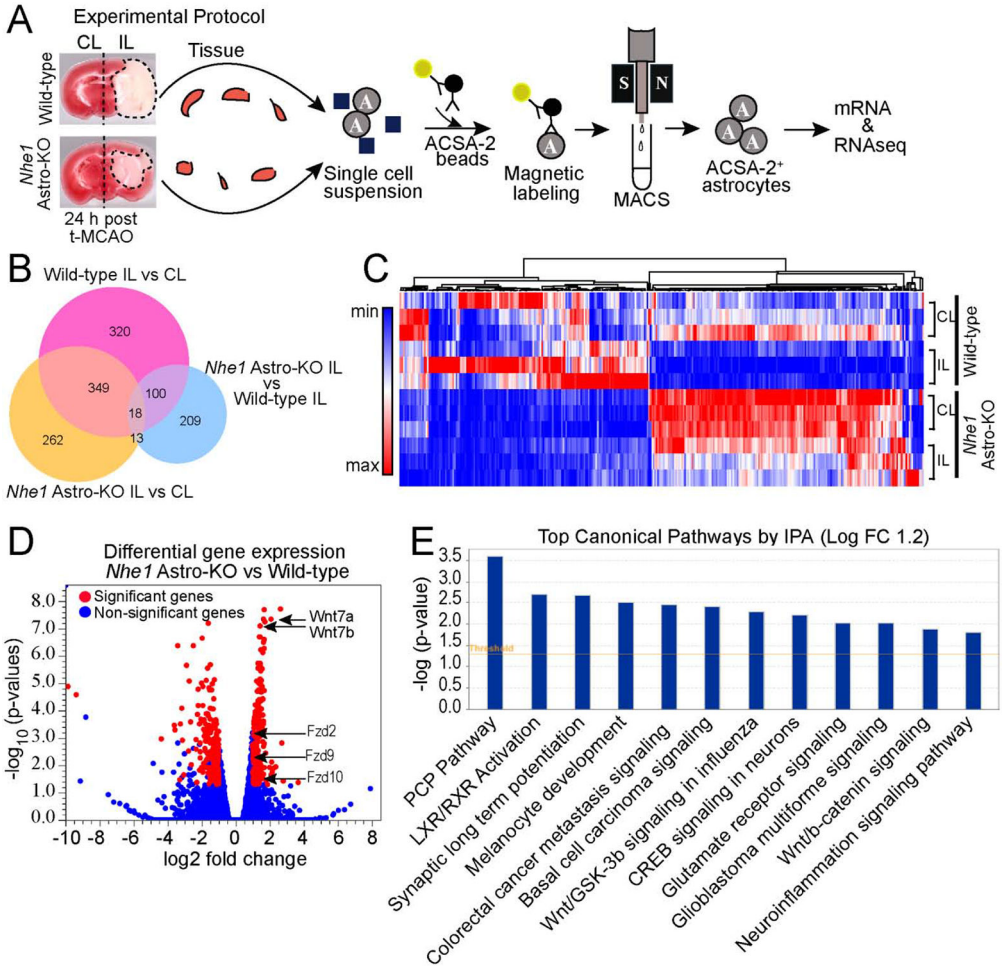

Fig. 3.

Bulk RNAseq analysis of transcriptome changes of wild-type and *Nhe1* Astro-KO astrocytes. (A) Schematics of bulk RNAseq analysisof astrocyte isolated from wild-type and *Nhe1* Astro-KOischemic brains at 24 h Rp. n=3. (B) Venn diagram depicting differential gene expression in astrocytes from wild-type and *Nhe1* Astro-KObrains (log2 fold change 1.2 and FDR p value < 0.05). (C) Heat map and unsupervised hierarchial clustering illustrates up-and down-regulated genes. (D) Volcano plots illustrates the gene expression pattern detected with log2 fold change 1.2 and an adjusted FDR p-value <0.05. (E) Significantly altered canonical pathways by Ingenuity pathway analysis (IPA).

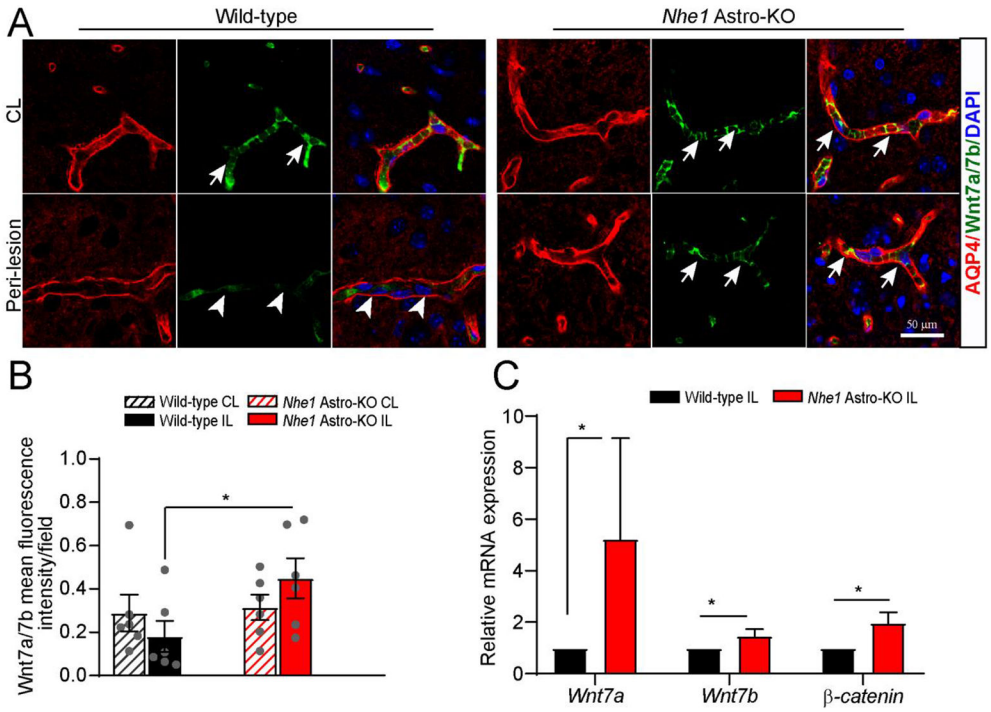

Fig. 4.

Nhe1 Astro-KO brains exhibited increased Wnt7a/7b expression. (A) Representative confocal images of AQP4+ and Wnt7a/7b+ positively stained vessels in wild-type and *Nhe1* Astro-KO ischemic brains at 48 h Rp. Arrows: high expression of Wnt7a/7b proteins. Arrowheads: low expression of Wnt7a/7b. (B)Bar graphs show quantification of Wnt7a/7b fluorescence signal intensity. Data are ± SEM, n=6. *p < 0.05 (Student's t-test). (C) RT-qPCR analysis of changes in expression of Wnt7a, Wnt7b, and β-catenin mRNA in the astrocytes isolated from wild-type and (A) Astro-KO brains at 24 h Rp. Data are mean ± SEM, n=4, *p < 0.05 (by Mann-Whitney Test). Representative confocal images of AQP4+ and Wnt7a/7b+ positively stained vessels in wild-type and *Nhe1* Astro-KO ischemic brains at 48 h Rp. Arrows: high expression of Wnt7a/7b proteins. Arrowheads: low expression of Wnt7a/7b. (B)Bar graphs show quantification of Wnt7a/7b fluorescence signal intensity. Data are ± SEM, n=6. *p < 0.05 (Student's t-test). (C) RT-qPCR analysis of changes in expression of Wnt7a, Wnt7b, and β-catenin mRNA in the astrocytes isolated from wild-type and *Nhe1* Astro-KO brains at 24 h Rp. Data are mean ± SEM, n=4, *p < 0.05 (by Mann-Whitney Test).

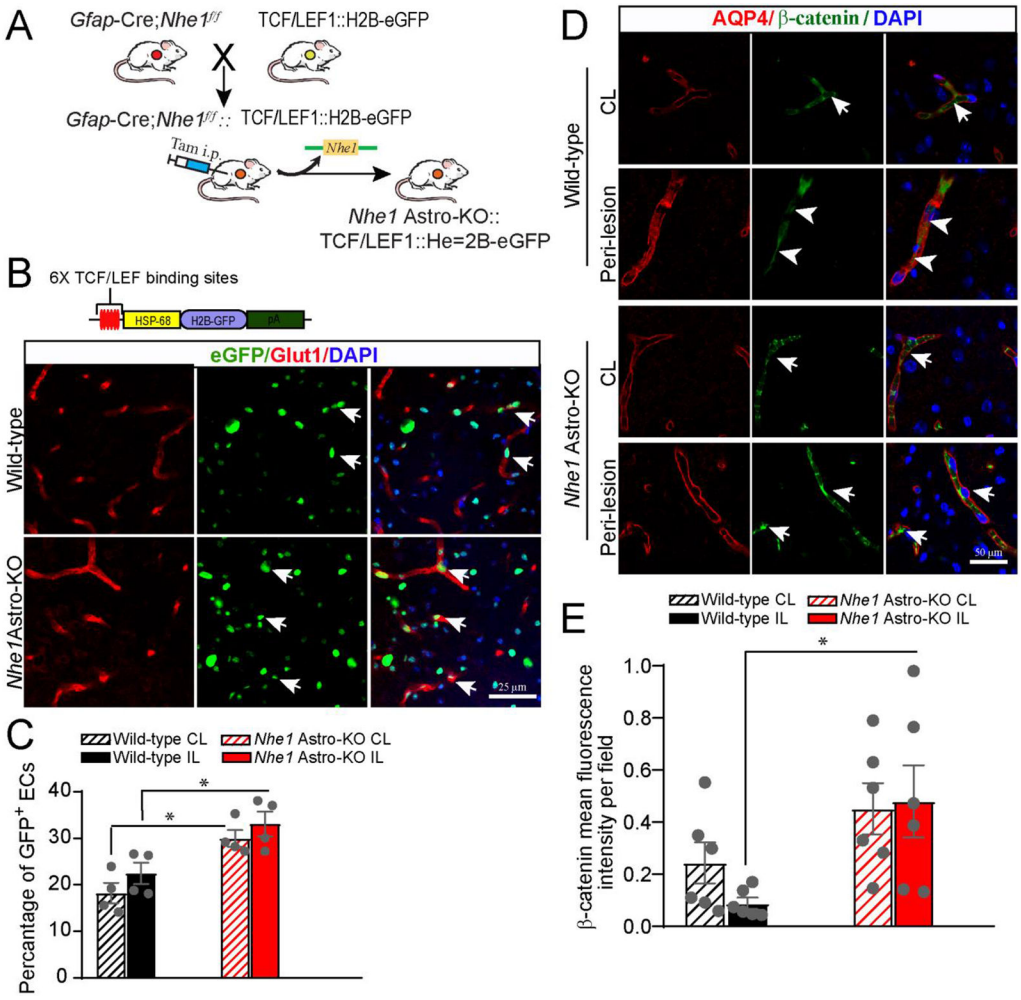

Fig. 5.

Elevated Wnt reporter transgene expression in wild-type and Nhe1Astro-KO brainsafter ischemic stroke. (A)Breeding scheme for generation of astrocyte specific Nhe1 KO mice containing the TCF/LEF1::H2B-eGFP Wnt reporter transgene. (B) Representative confocal images showing immunofluorescence for eGFP (green) and Glut1 (cerebral vessels; red) in the IL hemispheres of Nhe1 Astro-KO and wild-type reporter mice. (C) Quantification of Wnt reporter activity (eGFP immunofluorescence) in Glut1+ vessels. Data are mean ± SEM, n=4, *p<0.05 (two-way ANOVA for followed by Tukey's multiple comparisons test). (D) Repre-sentative images of AQP4 and β-catenin staining in the peri-lesion areas of wild-type and Nhe1 Astro-KO brains at 48 h Rp. Arrows: high expression of β-catenin protein. Arrowheads: Low expression of β-catenin. (E) Quantification of β-catenin staining intensity. Data are mean ± SEM, n = 5, *p < 0.05 (two-way ANOVA followed by Tukey's multiple comparisons test).

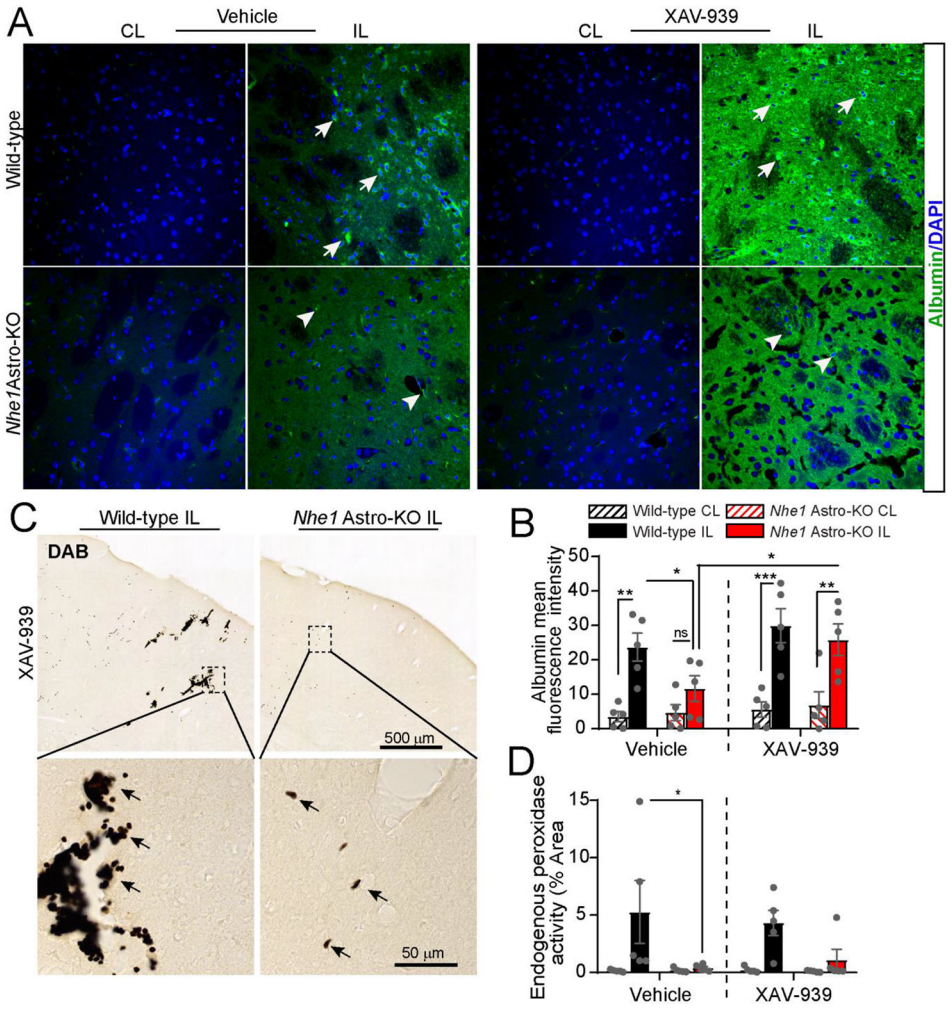

Fig. 6.

Pharmacological inhibition of Wnt/β-catenin signaling by β-catenin specific inhibitor XAV-939 abolished the BBB protection in Nhe1Astro-KO brains after ischemic stroke. (A) Representative confocal images showing albumin immunofluorescence staining in ischemic peri-lesion areas of wild-type and Nhe1 Astro-KO brains treated with vehicle and XAV-939 at 24 h Rp. (B) Summary of albumin infiltration. Albumin immunoreactivity was quantified by measuring the fluorescence intensity of images in panel A and B. Data are mean ± SEM, n = 5, *p < 0.05 (three-way ANOVA followed by Newman-Keuls multiple comparisons test). (C) Representative images of DAB-positive red blood cells showing the presence of intracerebral hemorrhages in the IL cortex of XAV-939 treated brains at 24 h Rp. (D) Quantification of the hemorrhagic percent area. Data are mean ± SEM, n = 5, *p < 0.05 (three-way ANOVA followed by Newman-Keuls multiple compari-sons test).

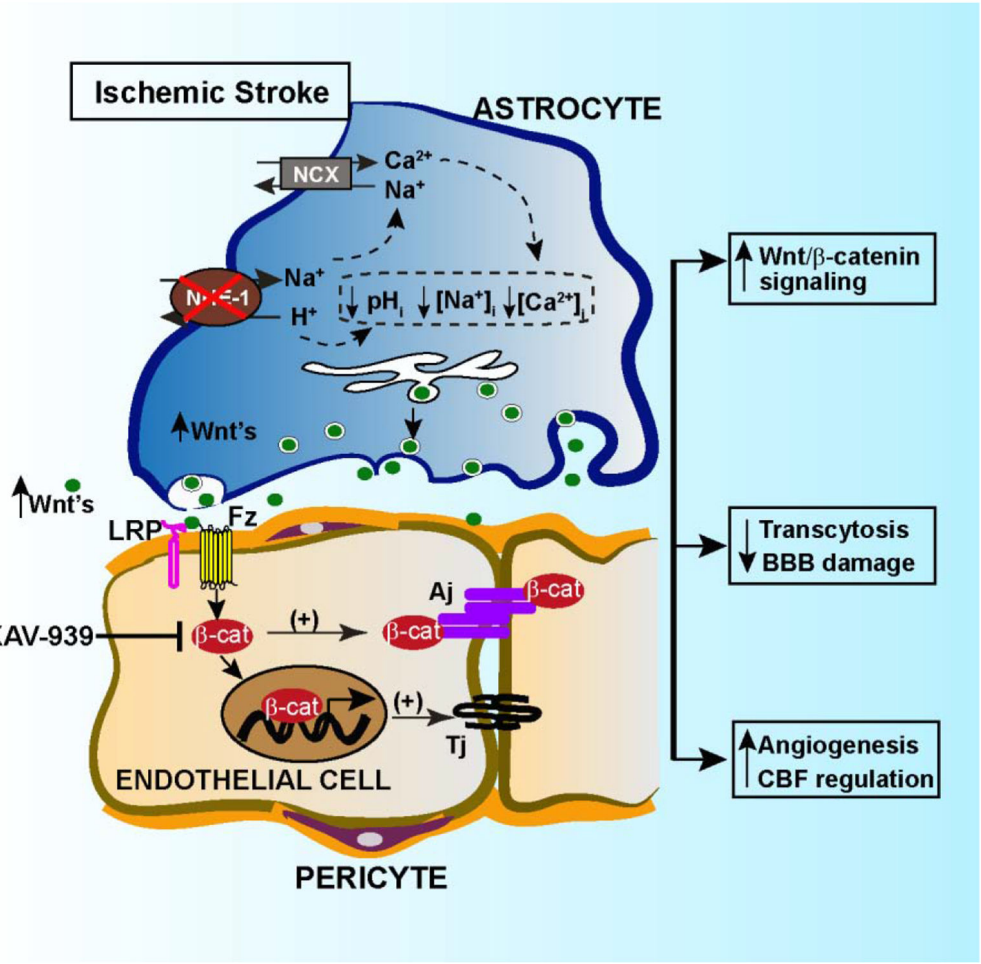

Fig. 7.

Mechanisms of astrocytic NHE1 in BBB damage in ischemic stroke.Ischemia stimulates NHE1 expression and activation in reactive astrocytes. Over-stimulation of NHE1 activity leads to pHi, and ion dysregultion. Selective deletion of astrocytic Nhe1 prevents NHE1 overstimulation, reduces BBB damage, and increases Wnt/β-catenin signaling in ECs, which promotes angiogenesis and improves rCBF.